Hindawi
Shock and Vibration
Volume 2018, Article ID 3239523, 21 pages
https://doi.org/10.1155/2018/3239523

Research Article

Study on Fatigue Degradation Behavior of a Cracked Rotor Subjected to Lateral Vibration

Qian Niu and Shi-xi Yang

College of Mechanical Engineering, Zhejiang University, Hangzhou 310027, China

Correspondence should be addressed to Shi-xi Yang; yangsx@zju.edu.cn

Received 28 April 2018; Accepted 7 July 2018; Published 29 August 2018

Academic Editor: Salvatore Caddemi

Copyright © 2018 Qian Niu and Shi-xi Yang. This is an open access article distributed under the Creative Commons Attribution License, which permits unrestricted use, distribution, and reproduction in any medium, provided the original work is properly cited.

Fatigue crack in a rotary shaft is a common failure observed in rotor systems. Since vibration of the shaft causes alternating fatigue loads, the crack propagates slowly. Meanwhile, the propagating crack may cause nonlinear or unstable vibration of the rotor system. In fact, growth of the crack and vibration of the shaft are coupled with each other. Hence, it is necessary to study the fatigue degradation behavior of the cracked rotor accounting for this coupling effect. In this paper, a coupling model of rotor vibration and crack growth is established through dynamic theory and fracture mechanics, and a sequential iterative procedure is proposed to solve the coupling model. Then, the competing degradation failure mode of the cracked rotor is analyzed with regard to the rapid crack growth failure and the unstable vibration failure. And degradation measures are proposed based on the competing degradation failure criterion. At last, degradation behaviors with the coupling effect of nonlinear vibration behavior and multiple parameters including rotation speed, unbalance eccentricity and orientation angle, and damping are investigated by numerical simulation. The results indicate that nonlinear vibration behavior and multiple parameters have considerable influence on the degradation behaviors, which present complex regularity. The findings are of significance to guide the safety design of the rotor system for long time operation and help to the further research on prognostics and lifetime prediction.

1. Introduction

Rotary machinery is a kind of common mechanical structure, which is widely used in industry equipments. Because of the rotary motion, the rotor suffers from the alternating fatigue loads. The initiation and further propagation of the fatigue crack are caused subsequently. The presence and propagation of the crack lead to nonlinear, complicated, or even unstable vibration behavior and the performance degradation of the rotor, which may cause severe damage to mechanical components or even catastrophic accidents.

Many researchers studied the modeling issues of cracked rotors and ulteriorly analyzed the characteristics of vibration behavior. Wauer gave a literature survey on the dynamics of cracked rotors published before 1990 [1]. Dimarogonas reviewed the research on vibration of cracked structures especially cracked rotors [2]. Papadopoulos reviewed the strain energy release approach for modeling cracks in rotors and vibration behavior of cracked rotors [3]. Kumar and Rostagi gave a brief review on various approaches for analyzing dynamic characteristics of cracked rotors [4]. Most studies are based on an assumption that the crack is relatively static; that is, the crack does not propagate or grow during the operation. Since the propagation of a crack is a much slower process than the vibration of the rotor, the above assumption is reasonable when studying the vibration behavior of the rotor during a short period of time. However, when assessing the performance degradation level of the cracked rotor, predicting the fatigue lifetime, conducting the Prognostic Health Management (PHM), and reliability analysis during a long period of the operation, it is required that not only the vibration behavior but also the crack growth behavior is properly addressed.

Crack growth causes slow decrease of the stiffness and variation of the dynamic characteristics of a cracked rotor system, which leads to fatigue degradation. During the slow

decreasing evolution, the stiffness also changes fast and periodically. Due to the weight and rotation of the rotor, the surface crack in the shaft opens and closes periodically, namely, the breathing effect, which causes the variation of the stiffness in every rotation period. Accounting for the breathing effect, the cracked rotor presents nonlinear vibration behavior. Some researchers focused their studies mainly on unbalance vibration responses of the nonlinear cracked rotor system [5–9] and the nonlinear vibration behavior due to the breathing effect of the crack, including bifurcation, quasi-periodic, and chaotic motions [10–16]. In engineering practice, the crack growth may lead to variation of the vibration behavior; for example, period-one motion may turn to bifurcation or quasi-periodic motion as the crack depth increases. The nonlinear vibration behavior may cause more complicated fatigue loads than the period-one response of constant amplitude. Therefore, when studying the crack growth behavior of a cracked rotor, the practical fatigue loads with respect to the vibration responses should be well addressed. However, when most researchers worked on the issues of the fatigue crack growth in shafts or round bars, the fatigue loads of constant or variable amplitudes were pregiven artificially or hypothetically, rather than the practical service loads in real applications [17–20]. In fact, the slow crack growth affects the fast rotor vibration behavior while the vibration affects the crack growth behavior. Hence, for a cracked rotor system, the slow process of crack growth and the fast process of rotor vibration are interactional and mutually coupled with each other.

Apparently, adequate models and approaches are required to account for both the fast rotor dynamics and the slow fatigue degradation of the fast-slow coupled system of the cracked rotor. Sobczyk and Trebicki provided general formulations for solving stochastic response-degradation coupled problem of structures with fatigue-induced stiffness degradation and presented the efficient sequential method for coupled response-degradation analysis [21]. Then, their approach was developed to analyze nonlinear stochastic vibratory systems with stiffness degradation [22] and multidimensional vibratory degrading systems [23]. Luo et al. proposed a model-based prognostic method and used the interacting multiple model to estimate the damage evolution of the coupled system under multiple operation modes [24, 25]. Lei and Zhu analyzed the crack growth behavior of the elastic element in nonlinear systems under random loads, accounting for the stiffness degradation caused by the crack growth [26].

However, the coupling models presented by Sobczyk, Luo, and Lei et al. are general ones or only for simple structures. In their study, the essential relationship between degradation measure (e.g., crack depth) and the system stiffness is directly given by experience. Moreover, the general models barely account for the specific characteristics and behavior of the cracked rotor system. Firstly, the dynamic behavior of the cracked rotor is influenced by multiple parameters of the system including not only stiffness but also rotation speed, unbalance eccentricity and orientation angle, and damping. The multiple parameters may have a complicated and coupling effect on the dynamic characteristics and hence the degradation behavior of the rotor system. Secondly, the only consideration of the stiffness degradation caused by crack growth is inadequate because the stiffness also presents periodic characteristic due to the breathing effect of the crack. The nonlinear vibration behavior induced by the breathing crack may have a remarkable impact on the degradation behavior. Thirdly, the crack growth disciplinarian of dynamic rotary shafts is more complicated than that of static simple structures, like bars and plates. Consequently, it is difficult to provide simplified experience formulas illustrating the complex relationship between the crack size and the system stiffness and the relationship between the vibration responses and the fatigue loads. These relationships are required to be revealed by corresponding physical models. Therefore, with all the above considerations, it is of great significance to establish a specific and applicable fast-slow coupling model of the cracked rotor and then to analyze the degradation behavior with the coupling effect of nonlinear vibration behavior and multiple parameters.

Moreover, before analyzing the degradation behavior of the cracked rotor, the degradation failure criterion and appropriate degradation measures are necessary to be addressed. Sobczyk and Trebicki defined degradation measure based on the crack depth, and fracture criterion was regarded as the degradation failure criterion [21, 22]. However, it may be inadequate since the degradation failure may occur before the crack grows to the critical depth due to severe or unstable vibration behavior. To insure the stability of the vibration, some researchers worked on the stability issues of the cracked rotor with multiple parameters [27–29]. Nevertheless, unstable vibration failure may not occur even if the crack grows over the critical depth in some cases. Therefore, the competing degradation failure modes caused by both rapid crack growth and unstable vibration should be well considered. Then, degradation measures should be properly proposed accounting for the competing degradation failure criterion. Moreover, the unstable vibration of the cracked rotor presents bifurcations of different types [29], which may have different influences on the degradation behavior.

The main objective of this article is twofold. One is to establish the fast-slow coupling model accounting for nonlinear dynamics of the cracked rotor and the fatigue propagation of the transverse surface crack. The other is to analyze the degradation behavior with the coupling effect of the nonlinear vibration behavior and the multiple parameters of the rotor system. Firstly, the coupling model of a Jeffcott rotor with a transverse surface crack is established based on dynamic theory and fracture mechanics. And a sequential iterative procedure is proposed to approximately solve the coupling model. Then, the degradation measure of the cracked rotor is defined based on the competing degradation failure criterion which accounts for both the unstable vibration of the rotor and the rapid growth of the crack. At last, the degradation

behaviors with the coupling effect of multiple parameters of the rotor system including rotation speed, unbalance eccentricity and orientation angle, and damping are analyzed through numerical simulation and several new findings are reported.

2. Problem Description

We consider a cracked rotor, depicted in Figure 1, modeled as a Jeffcott rotor system in which the rotor is simplified to a centered rigid disk on a massless elastic shaft and a transverse surface crack is located at the midspan of the rotor, which propagates as the shaft rotates. The initial of the crack is not considered in this study, and only the fatigue degradation behavior caused by the macroscopic crack growth is analyzed. For simplifying the analysis and calculation, several assumptions are made in this study:

(1) Torsional vibration and axial vibration of the shaft and shearing action are omitted. Only lateral vibration and crack growth under mode I are considered.

(2) The front of the crack is a straight line and maintained during the growth.

(3) The linear elastic fracture mechanics is employed for the analysis due to the applied stress being much less than the yielding stress.

(4) Only the plane strain condition is considered at the crack front due to the geometry constraint.

(5) The thickness of the disk is neglected, and the displacement at the crack location is the same as the disk.

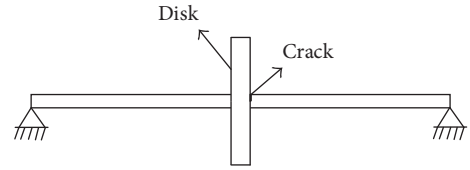

Figure 1: Schematic of the cracked rotor.

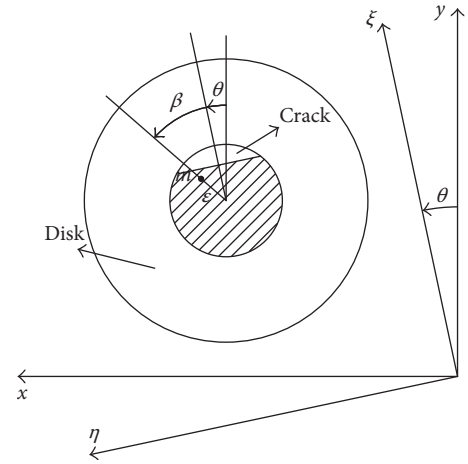

Figure 2: Coordinate system.

3. Model Establishment

The physical model of a Jeffcott rotor with a propagating surface transverse crack is established in two steps. Firstly, the dynamic model of the cracked rotor is established and then the crack growth model. The two models are coupled with each other due to the growing crack, which will be described in detail in this section. Noting that the main creative study focuses on the coupling effect of rotor dynamics and crack growth on the degradation behavior, the widely-used classical models of the cracked rotor and the crack growth are adopted for simplicity.

3.1. Vibration Differential Equations of the Cracked Rotor. The mass of the Jeffcott rotor m is assumed to be concentrated on the disk in the midspan. Let x-y be the fixed coordinates and $\xi - \eta$ be the rotating coordinates in the crack cross section as shown in Figure 2.

The unbalance eccentricity of the rotor is ε, which is oriented at an angle β (unbalance orientation angle) with the ξ coordinate direction. θ is the instantaneous angle of rotation at time t ($\theta = \omega t$), and ω is the rotation speed. c is the damping of the rotor system. Due to the existence of the crack, k_x and k_y are the stiffness of the x and y coordinate directions, respectively, and k_{xy} and k_{yx} are the cross stiffness. The dynamics of the rotor is combined by the translation of the centroid and the rotation around it. The dynamic equations for the cracked Jeffcott rotor can be written in the fixed coordinate system as

$$\begin{aligned} m\ddot{y} + c\dot{y} + k_y y + k_{yx} x &= m\varepsilon\omega^2 \cos(\theta + \beta) - mg, \\ m\ddot{x} + c\dot{x} + k_x x + k_{xy} y &= m\varepsilon\omega^2 \sin(\theta + \beta). \end{aligned} \tag{1}$$

The stiffness coefficients of (1) in the fixed coordinate system can be obtained from the stiffness coefficients k_ξ, k_η, $k_{\xi\eta}$, and $k_{\eta\xi}$ defined in the rotational frame $\xi - \eta$, by the transformation matrix $\mathbf{T}$:

$$\begin{bmatrix} k_y & k_{yx} \\ k_{xy} & k_x \end{bmatrix} = \mathbf{T}^{-1} \begin{bmatrix} k_\xi & k_{\xi\eta} \\ k_{\eta\xi} & k_\eta \end{bmatrix} \mathbf{T}, \tag{2}$$

where the transformation matrix $\mathbf{T}$ is

$$\mathbf{T} = \begin{bmatrix} \cos\theta & \sin\theta \\ -\sin\theta & \cos\theta \end{bmatrix}. \tag{3}$$

Cross section of the cracked rotor at the crack location is showed in Figure 3, where a is the depth of the crack, D is the diameter of the rotor, α' is the depth of the crack at the location where the η coordinate is w, and $\alpha' = \sqrt{D^2 - (2w)^2}$. The stiffness matrix is transformed from the flexibility matrix which can be derived by the strain energy release approach [3, 9, 16] (Appendix A). The flexibility coefficients of the cracked rotor can be derived as

$$g_\xi = \frac{L^3}{48EI} + \iint \frac{128L^2\alpha'^2\alpha^2}{E\pi D^8} F\left(\frac{\alpha}{\alpha'}\right)^2 d\alpha\, dw,$$

$$g_\eta = \frac{L^3}{48EI} + \iint \frac{512L^2w^2\alpha}{E\pi D^8} F'\left(\frac{\alpha}{\alpha'}\right)^2 d\alpha\, dw, \tag{4}$$

$$g_{\xi\eta} = g_{\eta\xi} = \iint \frac{256L^2\alpha' w\alpha}{E\pi D^8} F\left(\frac{\alpha}{\alpha'}\right) F'\left(\frac{\alpha}{\alpha'}\right) d\alpha\, dw.$$

It is worth noting that the integration limits in (4) depend on the open part of the crack which varies over time. On the one hand, the crack opens and closes periodically because of the breathing effect. One the other hand, since the crack propagates, the depth of the crack ($a(t)$) increases with time. Therefore, the integration limits in (4) depend on two aspects: the breathing effect and the propagation of the crack. Temporally, the propagation of the crack is omitted in this section, and only the breathing effect is considered, so the crack depth $a(t)$ becomes a. Several crack breathing models have been proposed, such as the harmonic model proposed by Mayes and Davies [1, 6, 30, 31], the crack closure line (CCL) model proposed by Darpe et al. [9, 16], and some new models with consideration of unbalance force [32]. In most applications, the gravity of the rotor is much larger than the unbalance force. In this situation, where the gravity is dominant, the harmonic model is appropriate and applied here. The stiffness matrix in the rotational frame is as follows:

$$\begin{bmatrix} k_\xi & 0 \\ 0 & k_\eta \end{bmatrix} = \begin{bmatrix} k_0 & 0 \\ 0 & k_0 \end{bmatrix} - F(\theta) \begin{bmatrix} \Delta k_\xi & 0 \\ 0 & \Delta k_\eta \end{bmatrix}, \tag{5}$$

where

$$F(\theta) = \frac{1}{2}\left[1 - \cos(\theta)\right], \tag{6}$$

$$\begin{aligned} \Delta k_\xi &= k_0 - \widehat{k}_\xi, \\ \Delta k_\eta &= k_0 - \widehat{k}_\eta, \end{aligned} \tag{7}$$

in which k_0 is the stiffness of the uncracked rotor, and $k_0 = 1/g_0$; $\widehat{k}_\xi$ and $\widehat{k}_\eta$ are the stiffness in the coordinate directions ξ and η when the crack is totally open. At fully open state of the crack, the flexibility coefficients $\widehat{g}_\xi$, $\widehat{g}_\eta$, and $\widehat{g}_{\xi\eta}$ can be calculated by (4), in which the integration region is the arched area of the open part of the crack. And the stiffness coefficients are

$$\begin{aligned} \widehat{k}_\xi &= \frac{\widehat{g}_\eta}{\widehat{g}_\xi\widehat{g}_\eta - \widehat{g}_{\xi\eta}^2}, \\ \widehat{k}_\eta &= \frac{\widehat{g}_\xi}{\widehat{g}_\xi\widehat{g}_\eta - \widehat{g}_{\xi\eta}^2}. \end{aligned} \tag{8}$$

Using (1)–(3) and (5)–(7), the equations of motion for the cracked rotor in a fixed frame x-y can be written as follows:

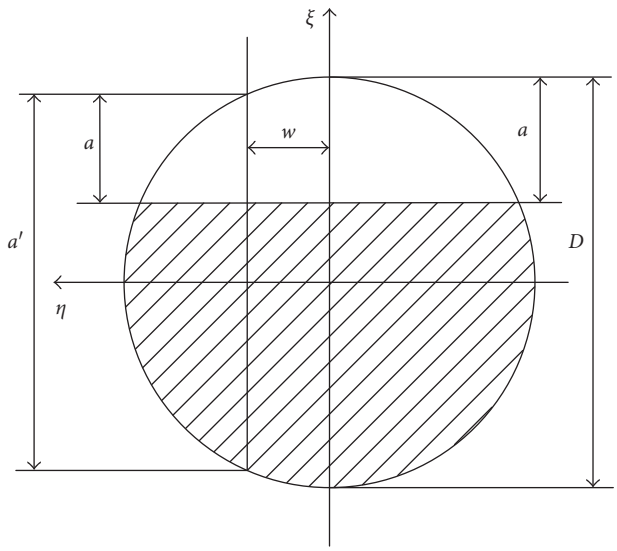

Figure 3: Cross-section at the crack location.

$$\begin{aligned} &m\ddot{y} + c\dot{y} + \left\{k_0 - 0.5F(\theta)\left[2k_0 - \widehat{k}_\xi - \widehat{k}_\eta + \left(\widehat{k}_\eta - \widehat{k}_\xi\right)\cos 2\theta\right]\right\} \\ &\quad \cdot y - 0.5F(\theta)\left[\left(\widehat{k}_\eta - \widehat{k}_\xi\right)\sin 2\theta\right]x = m\varepsilon\omega^2\cos(\theta + \beta) - mg, \\ &m\ddot{x} + c\dot{x} + \left\{k_0 - 0.5F(\theta)\left[2k_0 - \widehat{k}_\xi - \widehat{k}_\eta - \left(\widehat{k}_\eta - \widehat{k}_\xi\right)\cos 2\theta\right]\right\} \\ &\quad \cdot x - 0.5F(\theta)\left[\left(\widehat{k}_\eta - \widehat{k}_\xi\right)\sin 2\theta\right]y = m\varepsilon\omega^2\sin(\theta + \beta). \end{aligned} \tag{9}$$

It is important to note that stiffness coefficients in the dynamic model of the cracked rotor display periodic variation. And the period is equal to the rotation period T of the rotor, $T = 2\pi/\omega$. Furthermore, stiffness coefficients decrease slowly due to the growth of the crack, which will be illustrated in detail in Section 3.2. Therefore in real applications, stiffness coefficients in the dynamic model of the cracked rotor include two parts: the periodic part of fast variation and the decreasing part of slow variation. Consequently, the dynamic stiffness is a very complex function unable to be expressed in explicit formulations. The complex stiffness coefficients lead to complex vibration and degradation behaviors and bring difficulty to the solution of the dynamic model.

3.2. Propagation Equations of the Transverse Surface Crack. During the long time of operation, the transverse crack at the surface of the shaft grows slowly due to the fatigue stresses caused by the vibration of the rotor. The time history of the crack propagation is a very slow process, which can be regarded as the fatigue degradation evolution of the cracked rotor. A large majority of fatigue crack growth experiments on small specimens have shown that the fatigue growth of a crack in the metallic material is mainly controlled by the range of stress intensity factor (ΔK) of the crack front, although many factors, such as mean stress, load ratio and frequency, random loading, multiaxial and complex stress states as well as environments (corrosion and temperature), plastic zone, and microstructure, affect the manner of fatigue

crack growth. When ΔK is larger than the threshold of the fatigue crack growth (ΔK_{th}), the crack growth behavior can be described by the famous Paris–Erdogan laws [33, 34]:

$$\frac{da}{dN} = C(\Delta K)^B, \tag{10}$$

where a is the depth of the crack, N is the number of the stress cycles, and C and B are empirical parameters accounting for the material and environmental effects and in practice, can be obtained from small specimens by a regulated procedure, such as that proposed in ASTM E647-15 [35].

ΔK can be calculated by (A.5)–(A.9). The bending force acting on the crack cross section Q_ξ and Q_η can be calculated as follows:

$$\begin{aligned} Q_\xi &= k_\xi \xi + k_{\xi\eta}\eta, \\ Q_\eta &= k_\eta \eta + k_{\eta\xi}\xi, \end{aligned} \tag{11}$$

where the vibration responses ξ and η in the rotation frame can be obtained by a transformation from the rotor responses x and y in the fixed frame:

$$\begin{Bmatrix} \xi \\ \eta \end{Bmatrix} = \begin{bmatrix} \cos\theta & -\sin\theta \\ \sin\theta & \cos\theta \end{bmatrix} \begin{Bmatrix} y \\ x \end{Bmatrix}. \tag{12}$$

k_ξ, k_η, $k_{\xi\eta}$, and $k_{\eta\xi}$ are stiffness of ξ and η coordinate directions and crossing direction, respectively:

$$\begin{aligned} k_\xi &= \frac{g_\eta}{g_\xi g_\eta - g_{\xi\eta}^2}, \\ k_\eta &= \frac{g_\xi}{g_\xi g_\eta - g_{\xi\eta}^2}, \\ k_{\xi\eta} = k_{\eta\xi} &= \frac{-g_{\xi\eta}}{g_\xi g_\eta - g_{\xi\eta}^2}. \end{aligned} \tag{13}$$

From (A.6), one can conclude that the SIF at any location of the crack front is related to the local stress, the geometry size of the crack, and the specific position along the crack front. Therefore, ΔK at different locations is unequal, the same as the crack growth rates, which cause the change of the shape of the crack front. When the crack grows, the new shape of the crack front is only determined by the current crack front and has nothing to do with the initial crack front [19, 35]. In [33], it can be found that, under bending fatigue stress, the shape of the crack front tends to be a straight line as the crack grows to the center of the shaft. And many researchers assumed the crack front to be straight for simplification when studying cracked rotors [3, 36–38]. In this paper, for convenience of the analysis, it is assumed the crack front maintains straight when the crack grows.

Based on the assumption that the crack front maintains straight, an appropriate equivalent SIF is necessary to be defined to apply the Paris–Erdogan laws. In [39], the researchers derived an average SIF expression as an equivalent SIF from the SIF expressions of the edge and middle points of the crack front through Lagrange polynomial interpolation. In this study, in order to assure the safety of the rotor system, a conservative equivalent SIF is defined, which is the SIF of the point where the crack grows fastest. From [19, 40], regardless of the stress range $\Delta\sigma$, the SIF of the edge point is larger than that of the middle point. Moreover, in the condition of this study, it can be derived from (A.7) that the stress range $\Delta\sigma$ of the edge point is larger than that of the middle point. Therefore, ΔK at the edge point of the crack front is the largest, which means the crack at the edge point grows fastest, and the SIF of the edge point is chosen to be the equivalent SIF.

The edge point of the crack front actually refers to a point very close to the intersection of the crack front with the free surface of the shaft [19]. When the depth of the crack is a, the η coordinate of the edge point is $w = \pm\sqrt{aD - a^2}$, the crack depth rate α/α' converges to zero from the positive direction, and the limits of the functions F and F' are calculated as follows:

$$\lim_{\alpha/\alpha' \longrightarrow 0^+} F\left(\frac{\alpha}{\alpha'}\right) = \lim_{\alpha/\alpha' \longrightarrow 0^+} F'\left(\frac{\alpha}{\alpha'}\right) = 1.1220. \tag{14}$$

From (A.5)–(A.7), the equivalent SIF K_{e} is written as follows:

$$K_{\text{e}} = 1.1220\sigma_{\text{e}}\sqrt{\pi a}, \tag{15}$$

where σ_{e} is the equivalent stress and expressed as follows, which is the total stress at the edge point:

$$\sigma_{\text{e}} = \sigma_\xi + \sigma_\eta = \frac{L}{4I}\left[\left(\frac{D}{2} - a\right)Q_\xi + \sqrt{aD - a^2}\, Q_\eta\right]. \tag{16}$$

It is worth noting that the depth of the crack a is growing over time actually and should be written as $a(t)$. From (15) and (16), one can derive that the equivalent SIF K_{e} is dominant by the crack depth $a(t)$ which varies slowly and the equivalent stress σ_{e} which varies fast. Using (10), the crack depth a_N after N ($N = 1, 2, 3, \ldots$) stress cycles (or rotation periods) can be calculated by integration from the crack depth a_{N-1} as follows:

$$a_N = a_{N-1} + \int_{N-1}^{N} C\left(\Delta K_{\text{e}}(N)\right)^B dN, \tag{17}$$

where $\Delta K_{\text{e}}(N)$ is the range of the equivalent SIF in the Nth rotation period.

3.3. Solution of the Coupling Model. From Sections 3.1 and 3.2, the degrading cracked rotor system can be expressed as a hierarchical dynamic system form:

$$\dot{\mathbf{q}} = \mathbf{f}(\mathbf{q}, \boldsymbol{\mu}(\boldsymbol{\Phi})), \tag{18a}$$

$$\dot{\boldsymbol{\Phi}} = \nu\mathbf{g}(\boldsymbol{\Phi}, \mathbf{q}), \tag{18b}$$

where $\mathbf{q} = \begin{bmatrix} y & x \end{bmatrix}^T$ is a fast-time variable; $\boldsymbol{\Phi}$ is a slow-time variable and refers to the crack depth a in this study; $\boldsymbol{\mu}$ is a function of $\boldsymbol{\Phi}$ representing stiffness matrix; ν is a small rate constant which defines a time scale separation between fast and slow-time dynamics; and the overdot denotes differentiation with respect to time t. Over the time scales of $\mathrm{O}(\nu)$, we consider (18a) to be quasi-stationary since drifts in $\boldsymbol{\mu}$ are negligible.

The rotor vibration equations and the crack propagation equations are coupled with each other, forming the vibration-degradation coupling model. Since it is difficult to describe the function $\boldsymbol{\mu}$ and $\mathbf{g}$ by explicit function expressions, the customary approximate analytic procedures cannot be applied to solve the coupling model. Alternatively, a numerical procedure is proposed here, which is based on sequential iteration. In engineering applications, the crack grows very slowly compared to the natural time scale of the rotor vibration process. It means that the crack depth can be regarded as constant in a short time interval. In this study, it is assumed that the crack depth a_{M-1} is constant in n rotation periods (time interval nT), and after n periods, the crack depth grows to a_M. Based on this assumption, the stiffness coefficients of the vibration equations dominated by the crack depth can be calculated in the time interval of n rotation periods, and vibration differential equations (9) can be solved through various existing analytic or numerical procedures. The solutions of (9) are vibration responses $(x(t), y(t))$ of the cracked rotor and are used to calculate the time history $K_{eM}(t)$ $(t_{M-1} < t < t_M)$ by (11)–(16). Then, using (17), a_M is calculated as follows:

$$a_M = a_{M-1} + \int_{M-1}^{M} C\left(\Delta K_{eM}(N)\right)^B dN, \tag{19}$$

where $\Delta K_{eM}(N)$ denotes the SIF range of the Nth rotation period, which is dependent on $K_{eM}(t)$. At last, given the initial crack depth a_0, the crack growth process described by the crack depth a_M $(M = 1, 2, 3, \ldots)$ of each time interval can be obtained by the iteration procedure.

It is worth noting that $K_{eM}(t)$ is determined by $x(t)$ and $y(t)$ in the time interval $t_{M-1} < t < t_M$. When the vibration of the rotor is period-one motion, the amplitude of each period is equal. Therefore, $\Delta K_{eM}(N)$ of every rotation period is also the same, and in this situation, (19) can be written as follows:

$$a_M = a_{M-1} + nC\left(\Delta K_{eM}(N)\right)^B. \tag{20}$$

However, when the vibration behavior of the cracked rotor is complex, such as bifurcation motion, quasi periodic motion, and chaotic motion [10–16], $K_{eM}(t)$ of each rotation period is not the same anymore. In this situation, a statistical counting method is necessary to be applied to count $\Delta K_{eM}(N)$ from $K_{eM}(t)$. In this study, the rain-flow counting method [41, 42] is applied which is widely used in research and real applications. Then, the integration part of (19) can be calculated.

4. Degradation Measures

To evaluate the degradation level and analyze the degradation behavior, quantitative degradation measures are necessary to be proposed. Moreover, the definition of degradation measures is associated with the threshold of the degradation failure or the so-called failure criterion. For the cracked rotor system, a competing degradation failure criterion is described in detail in this section.

4.1. Degradation Failure Criterion of the Cracked Rotor. If one wants to define the degradation measure of the cracked rotor, a clear identification of failure criterion is needed. In [39], two failure criteria are considered: (1) geometrical limit: the failure occurs automatically when crack depth is larger than shaft diameter and (2) critical SIF: the fracture occurs when maximum SIF is larger than critical SIF. However in engineering applications, the fracture of the rotor is not allowable in most cases. The rotor should maintain a safe and stable running state. Once the running state becomes risky or unstable, the inspection or maintenance is required. Detecting the dangerous and unstable running states as soon as possible is of great significance, which is an important objective of condition monitoring and prognostics. Obviously, it is unsafe and inappropriate to regard the fracture criterion of the shaft as the degradation failure criterion of the rotor system. That is why the safe factor is necessary in engineering applications.

Fatigue experiments illustrate that the crack grows rapidly at increasing growth rate greater than that of the Paris law in a short period time before maximum SIF reaches critical SIF [19]. Consequently, a critical crack depth for rapid crack growth (notated as a_c) can be defined through experiments or experience. Once the crack grows deeper than a_c, rapid and unstable crack growth occurs. Although fracture does not occur during the time of rapid and unstable crack growth, the running state of the rotor system is risky. Therefore, in this study, a degradation failure criterion based on the growth of crack is defined as $a > a_c$.

Moreover, for the vibration behavior of the cracked rotor, unstable vibration occurs when the crack depth reaches some thresholds for some rotation speeds [29], which is undesirable in real applications. The situation possibly exists, in which unstable vibration occurs before the crack depth reaches a_c. Thus, it is necessary to address the condition on which unstable vibration occurs. In Section 3.3, it is assumed that the crack depth is constant in the short time interval of nT. In this situation, the stiffness coefficients of the cracked rotor system vary periodically, and Floquet's theory is applicable for stability analysis [43–45] (Appendix B).

Once Floquet multipliers exceed the unit circle on the complex plane, the vibration of the cracked rotor system becomes unstable and bifurcation occurs. As shown in Figure 4, different distributions of the Floquet multipliers on the complex plane correspond to different types of bifurcations. There are three types of bifurcations: fold (period doubling), Hopf, and flip (saddle-node), as shown in Figure 4 [29, 37]. When even small damping (e.g., damping ratio $\zeta = 0.01$) exists, the unstable region corresponding to Hopf bifurcation vanishes [37]. Since damping surely exists in engineering applications, only fold and flip are considered in this study.

As to period-doubling bifurcation, vibration amplitude does not increase suddenly. In this situation, degradation failure does not occur to the cracked rotor since the vibration amplitude is not overlarge. As to saddle-node bifurcation, vibration amplitude increases suddenly because of the divergence of the vibration responses. In this situation,

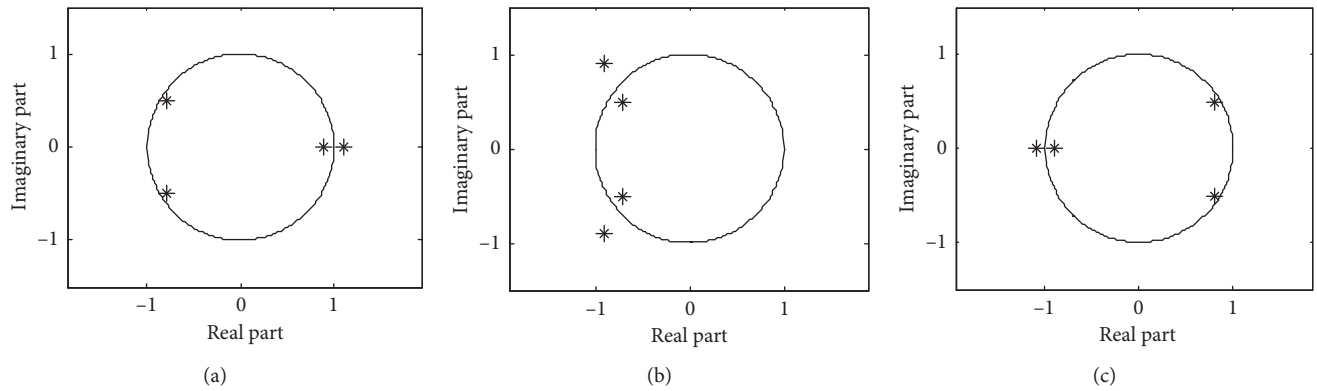

Figure 4: Eigenvalues on the complex plane corresponding to the three types of bifurcation: (a) fold; (b) Hopf; (c) flip.

degradation failure occurs, even if the crack depth has not reached a_c. When the vibration behavior reaches the boundary of the unstable region corresponding to the saddle-node bifurcation, the crack depth at this time is regarded as a critical crack depth for unstable vibration (notated as a_u). Given the necessary parameters in (9) including mass, damping, unbalance eccentricity and orientation angle, and rotation speed, one can address a_u under this parameter group through Floquet's theory. Accordingly, another degradation failure criterion based on vibration behavior is defined as $a > a_u$.

In conclusion, two degradation failure criteria of the cracked rotor are defined based on the crack growth and the rotor vibration, respectively. If one criterion is reached, the degradation failure occurs. Thus, a competing degradation failure criterion is formed.

It is worth noting that when the vibration of the cracked rotor is period-one motion, the coupling model can be solved by (20). However, when bifurcation occurs, the rain-flow counting method is acquired to calculate the integration part of (19).

4.2. The Proposed Degradation Measure. To define degradation measures, the competing degradation failure criterion accounting for both rapid crack growth and unstable vibration response are considered. According to [21], the degradation measure D $(0 \le D \le 1)$ is defined based on the evolution of crack growth. When the crack depth is zero, D equals 0, which means no crack exists. When the crack depth reaches a_c or a_u, D equals 1, which means degradation failure occurs. When the crack depth is a_M, the degradation measure is written as D_M and calculated as follows:

$$D_M = \frac{a_M}{\min\left(\left[a_c a_u\right]\right)}. \tag{21}$$

Furthermore, the average degradation rate at this time is defined as follows:

$$V_M = \frac{D_{M+1} - D_M}{n}. \tag{22}$$

It is assumed that there is already macroscopic initial crack on the surface of the shaft. The depth of the initial crack is assumed to be a_0 and the initial degradation measure is D_0 from (21). The fatigue degradation life T_D is defined as the number of stress cycles (or rotation periods), during which the cracked rotor degrades from D_0 to 1. If $D_M = 1$, $T_D = nM$.

5. Numerical Simulation and Parametric Sensitivity

5.1. Procedure and Parameters of Numerical Simulation. The degradation behavior of the cracked rotor described by the proposed coupling model is addressed by numerical simulation in this study, and the procedure is as follows:

(1) Given the initial crack depth and necessary parameters of the coupling model, the stiffness matrix of the cracked rotor is calculated using (4)–(8). Then, the Floquet multipliers under this parameter group are calculated according to Appendix B.

(2) Based on Floquet's theory and the distribution of the Floquet multipliers on the complex plane, the vibration state of the cracked rotor is indentified. If the vibration state is stable or period-doubling bifurcation, go on to the next step. If the vibration state is the saddle-node bifurcation, it means degradation failure occurs and the computation stops. The crack depth at this time is the critical depth for unstable vibration (notated as a_u).

(3) The steady-state responses of the vibration differential equations are derived by the Runge–Kutta fourth order numerical integration method. Then, using (11)–(16), $K_e(t)$ of n rotation periods of time is calculated. The new crack depth after growth is derived by (19). If the vibration state is stable, (20) is used. If not, the rain-flow counting method is applied to get $\Delta K_{eM}(N)$.

(4) Judge whether the new crack depth reaches the given critical depth for rapid crack growth (notated as a_c). If so, it means degradation failure occurs and the computation stops. If not, go back to step 1, and continue the computation using the new crack depth until degradation failure occurs.

In order to insure the veracity and reliability of the proposed model and simulation, the classical and validated models and theory are adopted, such as the harmonic model for the breathing effect, Paris's law for the crack growth, Floquet's theory for the stability analysis, and so on. Moreover, some intermediate results of the proposed simulation are compared to that of the published literatures, which is illustrated in Section 6.

Physical rotor parameters used for the simulations are as follows: shaft diameter, $D = 0.045$ m; length, $L = 0.7$ m; disk mass, $m = 25$ kg; and Young's modulus, $E = 2.1 \times 10^5$ MPa, referring the cracked rotor system in [16]. The empirical parameters used in the Paris–Erdogan laws are as follows: $C = 6 \times 10^8$, $B = 3$, referring to the crack growth model in [39]. The other parameters including unbalance eccentricity ε and orientation angle β and damping factor ζ are analyzed in detail in the following sections.

For different rotary shafts, physical rotor parameters such as shaft diameter, length, and mass are determined by the design scheme or can be directly measured in real applications. Young's modulus E and the parameters B and C used in the Paris–Erdogan laws are material related, which can be chosen according to the prior knowledge about the shaft material. Besides, without any prior knowledge, they can be measured by the experiment [20, 34, 46]. The other parameters which are difficult to measure directly, such as unbalance eccentricity, damping factor, and initial crack size, can be estimated through the off-line experiment or online measured data by various parameter identification methods, such as the least squares method and the maximum likelihood method [47–49]. Since the parameter measurement and identification are not the key point in this study, they are not introduced in detail and interested readers can refer to the literatures listed above.

Table 1: The concerned parameters and their global sensitivities.

	Ω	ε	β	ζ
Range	[1000,10000]	[0.5,2]	$[0,\pi]$	[0.01,0.05]
Unit	rpm	$\times 10^{-5}$ m	rad	—
Sensitivity	1.56	0.98	0.46	0.05

It is assumed the time interval is $n = 10^3$ rotation periods, during which the crack depth is constant. Floquet multipliers are computed with the time interval $K = 50$ and the order of Taylor expansion $N_l = 4$. Given crack depth a, the crack depth ratio $r = a/D$. It is assumed the initial crack depth $r_0 = 0.1$ ($r_0 = a_0/D$), and the critical depth for rapid crack growth $r_c = 0.5$ ($r_c = a_c/D$).

5.2. Parametric Sensitivity Analysis. Parametric sensitivity analysis is important to the system model analysis. It helps to know which parameter is more sensitive to the system output. In this study, four parameters are of interest, namely, rotation speed Ω, unbalance eccentricity ε and orientation angle β, and damping factor ζ, and the concerned system output is fatigue degradation life T_D. According to the research in [19], the concerned parameter ranges and corresponding unit are listed in Table 1.

Given a parameter space H^n of n dimensions, the local sensitivity of the system to a parameter p_i ($i = 1, 2, \ldots, n$) is defined as the partial derivative of the system function with respect to the parameter. According to [50], the local sensitivity of p_i to T_D about a nominal point p^* in the parameter space is calculated as

$$S_i^L(p^*) = \frac{T_D(p_1^*, \ldots, p_{i-1}^*, p_i^* + \Delta p_i^*, p_{i+1}^*, \ldots, p_n^*) - T_D(p^*)}{\Delta p_i^*} \times \frac{p_i^*}{T_D(p^*)}, \tag{23}$$

where Δp_i^* is the small increment in the parameter of interest.

Since the global sensitivity analysis accounts for interactions between variables and does not depend on the choice of a nominal point, it is adopted in this study. The grid resolution of the parameter space is ten grid points in each parameter axis, and 10^4 points are used to calculate global sensitivities. Based on a finite summation technique [50], the global sensitivity of p_i to T_D is calculated as

$$S_i^G = \frac{1}{m} \sum_{k=1}^{m} S_i^L(p^k), \tag{24}$$

where p^k represents the kth point in H^n and $m = 10^4$ is the total number of points in H^n. The global sensitivities of the interested parameters are shown in Table 1. The most sensitive parameter is rotation speed, which means the rotation speed is more influential to the degradation life than other parameters. The second sensitive parameter is unbalance eccentricity, which is more sensitive than the corresponding unbalance orientation angle. The least sensitive parameter is the damping factor. Notably, small global sensitivity does not mean a parameter is not important because its local sensitivity may be large about some possible points in the parameter space.

Since global sensitivity only presents the overall and general influence of a parameter to the system, we also need to know the specific and detailed influence of multiple parameters on the degradation behavior. The degradation behavior of the cracked rotor is studied by using degradation measure D, fatigue degradation life T_D, and average degradation rate V_M. Different influences of multiple parameters (rotation speed, unbalance eccentricity and orientation angle, and damping) are investigated in detail in Section 6.

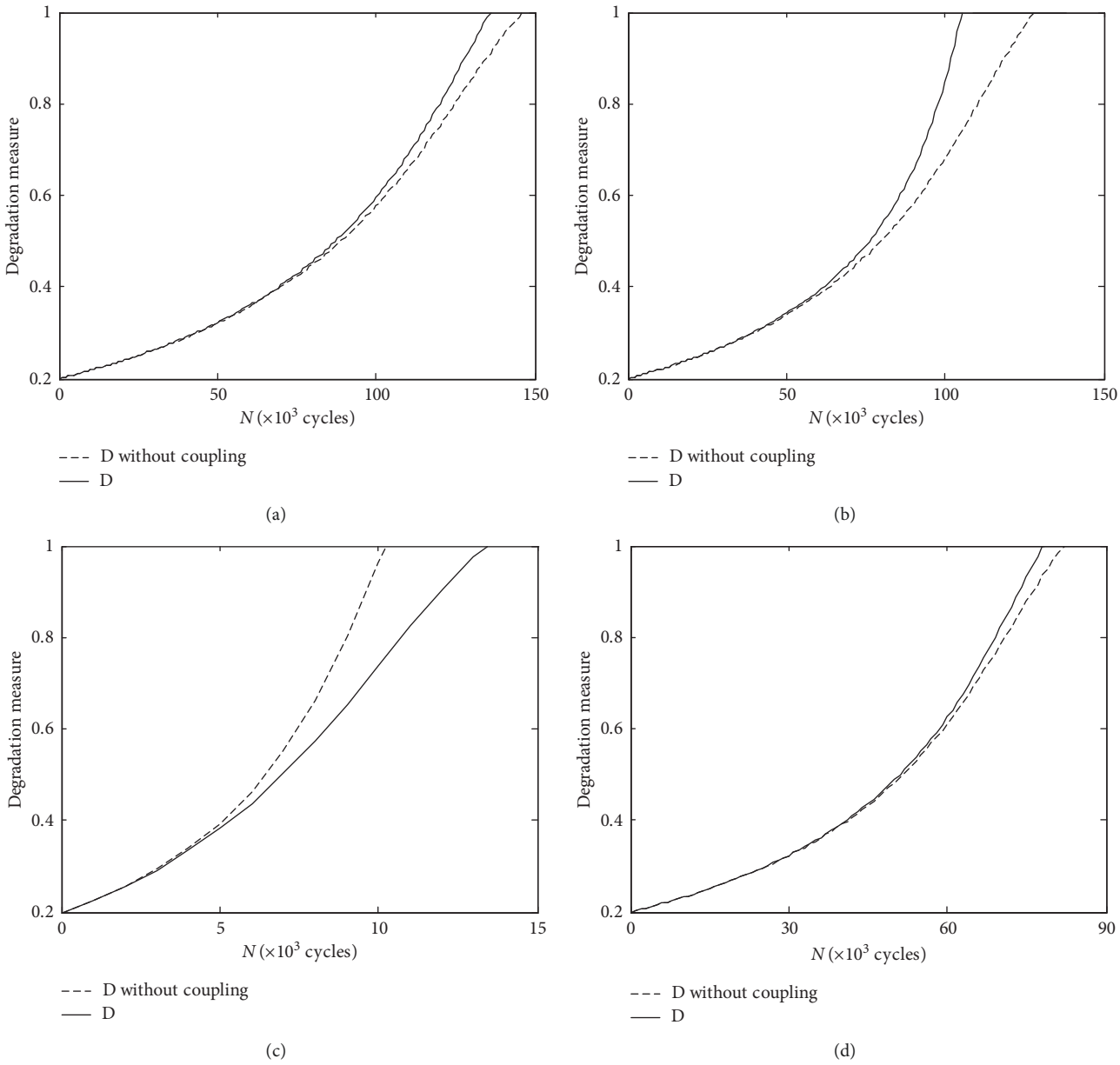

Figure 5: Degradation evolution presented by different degradation measures for different rotation speeds: (a) 1000 rpm; (b) 3000 rpm; (c) 5000 rpm; (d) 7000 rpm.

6. Results and Discussion

Given a specific rotation speed, the degradation evolution of the cracked rotor is computed, which is characterized by the degradation measure D. As comparison, the degradation evolution of the cracked rotor model omitted the coupling of the vibration response, and crack growth is also presented by the degradation measure D. Without accounting for the coupling effect, the vibration response of the initial state is used to calculate the crack growth. In particular, given the unbalance eccentricity $\varepsilon = 1 \times 10^{-5}$ m, unbalance orientation angle $\beta = 0$, and damping factor $\zeta = 0.01$ ($\zeta = c/2\sqrt{k_0 m}$), the degradation evolutions for rotation speed $\Omega = 1000$ rpm, 3000 rpm, 5000 rpm, and 7000 rpm are shown in Figures 5(a)–5(d), respectively, where the degradation time is presented as number of stress cycles.

As shown in Figures 5(a), 5(b), and 5(d), the degradation measure D with the coupling effect considered reaches 1 for less number of cycles than D without coupling, which means the degradation is slower if the coupling effect is omitted. This phenomenon is in agreement with the result of [21]. As to a linear system, magnitude of vibration response increases gradually as stiffness of the system decreases, which leads to the acceleration of degradation. However, as to the nonlinear cracked rotor system, magnitude of vibration response may decrease as stiffness of the system decreases for some specific parameter group. The nonlinear breathing effect of the crack may destroy or weaken the mechanism by which rotational

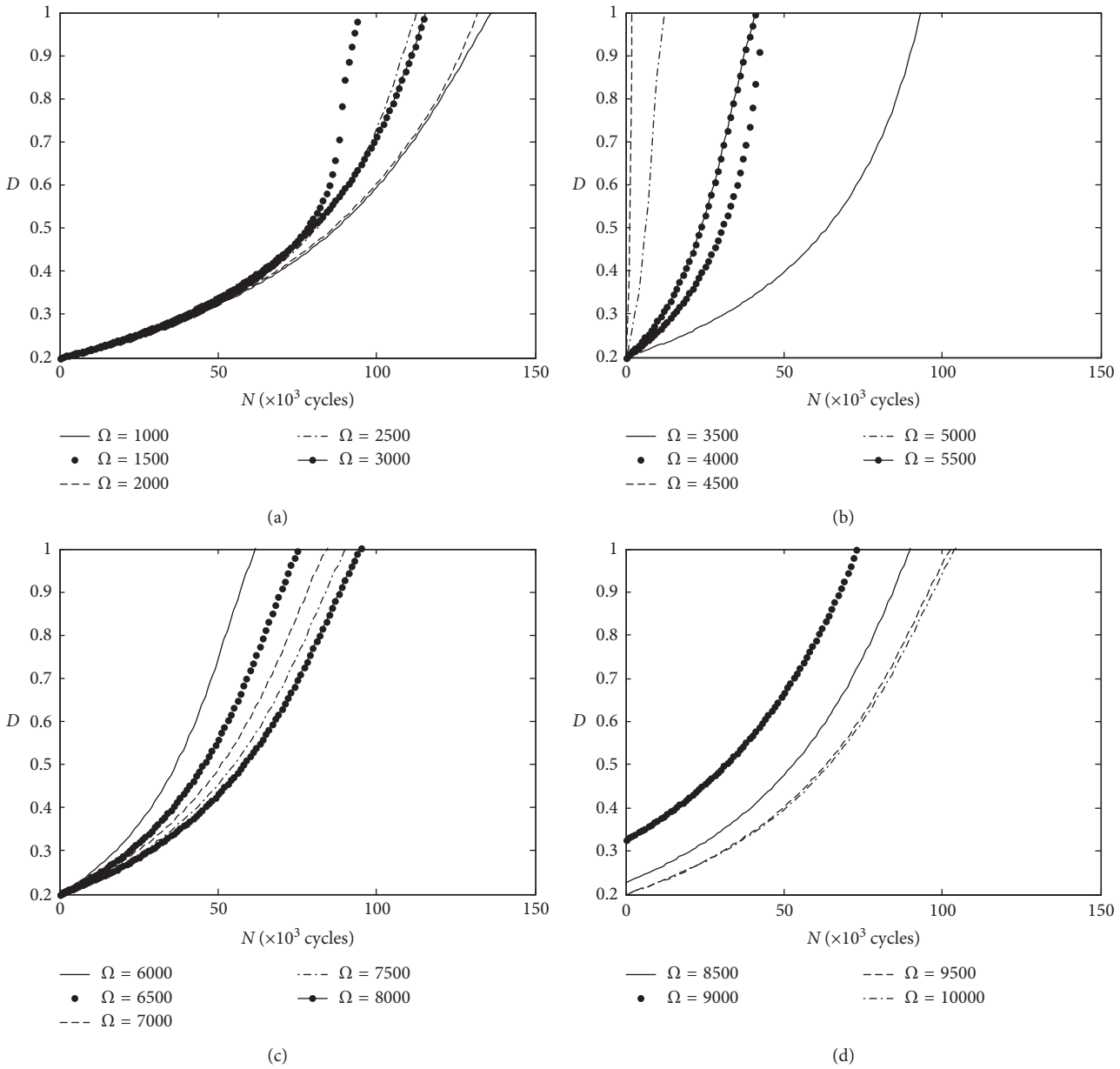

Figure 6: Degradation evolutions for various rotation speeds.

energy is transformed into transverse vibrational energy, which slows down the degradation, as shown in Figure 5(c). This phenomenon of the decrease in vibration amplitude as crack propagation has been reported in [51]. In engineering applications, underestimating the degradation rate may cause risky accidents, while overestimating the degradation rate can lead to a waste of maintenance resources. Therefore, when performing the fatigue design or using physics-based method to prognostic or predict residual life, the coupling effect cannot be omitted.

6.1. Effect of Rotation Speed. For the uncracked rotor, the first order critical rotation speed can be calculated using the stiffness of the uncracked rotor, as $\Omega_0 = 60\sqrt{k_0/m}/2\pi = 4645$ rpm. The simulations in this study run over the speed range 600 rpm–10000 rpm, which covers the double of the critical speed ($2\Omega_0 = 9290$ rpm). Given the parameters $\varepsilon = 1 \times 10^{-5}$ m, $\beta = 1/2\pi$, and $\zeta = 0.01$, the degradation evolutions for different rotation speeds (1000 rpm–10000 rpm with increment 500 rpm) are shown in Figure 6, where the degradation evolutions are characterized by the degradation measure D.

As Figure 6 shows, the degradation rate increases as the crack growth and the degradation evolution can be approximately depicted by the exponential function. For some rotation speeds, the degradation is obviously faster than others, like the degradation evolution for 1500 rpm, 4500 rpm, and 9000 rpm. However, there is no intuitive monotonous regularity for degradation evolutions as

rotation speed increases. In fact, since the degradation of the cracked rotor may be influenced by multiple factors, such as unbalance eccentricity ε and orientation angle β and damping factor ζ, a simple regularity controlled by a single factor is definitely not adequate to illustrate the degradation behavior.

Given $\varepsilon = 1 \times 10^{-5}$ m, $\beta = 1/2\pi$, and $\zeta = 0.01$, the fatigue degradation lifes T_D for different rotation speeds are shown in Figure 7. T_D does not change monotonously with speed but has several valleys. Specifically, when the rotation speed Ω is around 4600 rpm, T_D is of very few cycles, which means degradation failure occurs very fast. 4600 rpm is almost the critical speed noting that the critical speed of the cracked rotor is a little less than that of the uncracked rotor due to the decrease of stiffness. Therefore, the resonance causes the large amplitude of the vibration response and furthermore the fast degradation. When the rotation speed is around 1100 rpm, 1500 rpm, and 2300 rpm, which are the submultiples (1/2, 1/3, and 1/4) of the critical speed, T_D also decreases. The reason is that subharmonic resonance occurs [16] and causes the acceleration of degradation. This phenomenon of fast degradation gradually vanishes as speed decreases.

However, 2900 rpm (almost 2/3 of the critical speed) is far away from the resonance and subresonance region, around which T_D also has a small valley. The reason is that unstable vibration occurs at this parameter group if damping is very small [52, 53]. And the bifurcation causes the fast degradation, which will be verified in the following part.

When the rotation speed is around 9100 rpm (almost the double of the critical speed), T_D decreases and the initial degradation measure D is not 0.2 (Figure 6(d)). In this situation, degradation failure occurs owing to unstable vibration (saddle-node bifurcation) before the crack grows to the critical depth for rapid crack growth ($r_c = 0.5$). As shown in Figure 8, when the rotation speed is 9000 rpm, once the crack depth ratio reaches 0.32, the crack grows rapidly and failure occurs due to unstable vibration. The crack depth ratio 0.32 responds to the critical crack depth for unstable vibration (notated as a_u). Similarly, when the rotation speed is 8500 rpm, failure occurs at $r = 0.43$.

Given $\varepsilon = 1 \times 10^{-5}$ m, $\beta = 1/2\pi$, and $\zeta = 0.01$, the 3D and 2D color graphs of the average degradation rate V_M versus crack depth ratio and rotation speed are presented in Figure 9. It is observed that the rotation speeds around which V_M is relatively large are coincided with the valleys of T_D shown in Figure 7. These rotation speeds are the critical speed (4600 rpm), double (9100 rpm) and submultiples (1100 rpm, 1500 rpm, and 2300 rpm) of the critical speed, and 2/3 of the critical speed (2900 rpm), respectively. The regions of relatively large V_M around the critical speed and double of it are well coincided with the unstable vibration regions of the cracked rotor with small damping [27, 37, 47, 48]. However, it is worth noting that, around the critical speed, V_M increases gradually while around double of the critical speed, V_M increases abruptly when the crack depth reaches some threshold. The reason is that, around the critical speed, the cracked rotor reaches

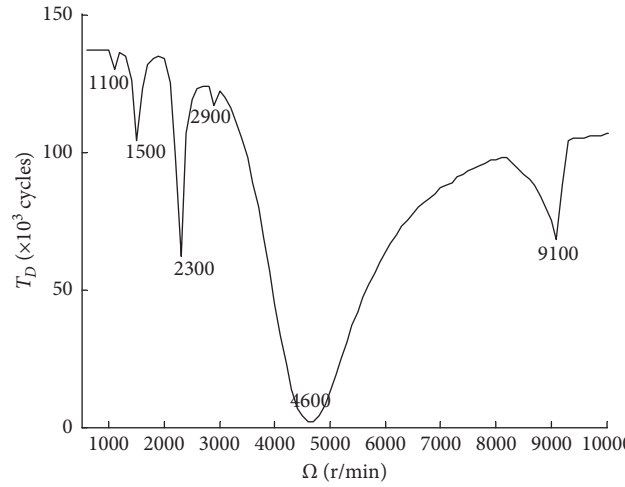

Figure 7: Fatigue degradation life versus rotation speed with $\varepsilon = 1 \times 10^{-5}$ m, $\beta = 1/2\pi$, and $\zeta = 0.01$.

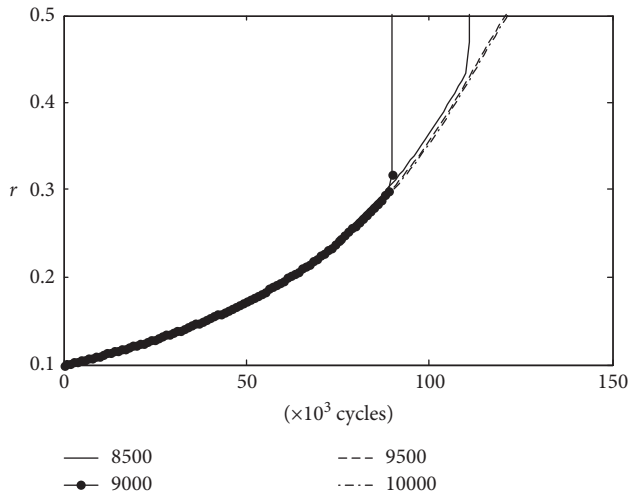

Figure 8: Crack growth evolutions for various rotation speeds.

the unstable vibration region through period-doubling bifurcation, in which case the response amplitude increases gradually as the crack grows. However, around double of the critical speed, the cracked rotor reaches the unstable vibration region through saddle-node bifurcation, in which case the divergence of vibration response occurs abruptly when the crack grows to some threshold depth. The Floquet multipliers for 4000 rpm–4600 rpm and 8000 rpm–9100 rpm with the crack depth rate changing from 0 to 0.5 are plotted in Figures 10(a) and 10(b), respectively, which illustrate the two different types of bifurcation. Besides, around 2900 rpm and $r = 0.45$, V_M is also relatively large, which is responsible for the valley of T_D at 2900 rpm in Figure 7. The bifurcation occurs at this parameter group as shown in Figure 11. The response amplitude of the y coordinate direction presents a larger variation around rotation speed 2900 rpm (Figure 11(a)) and around crack depth rate 0.45 (Figure 11(b)).

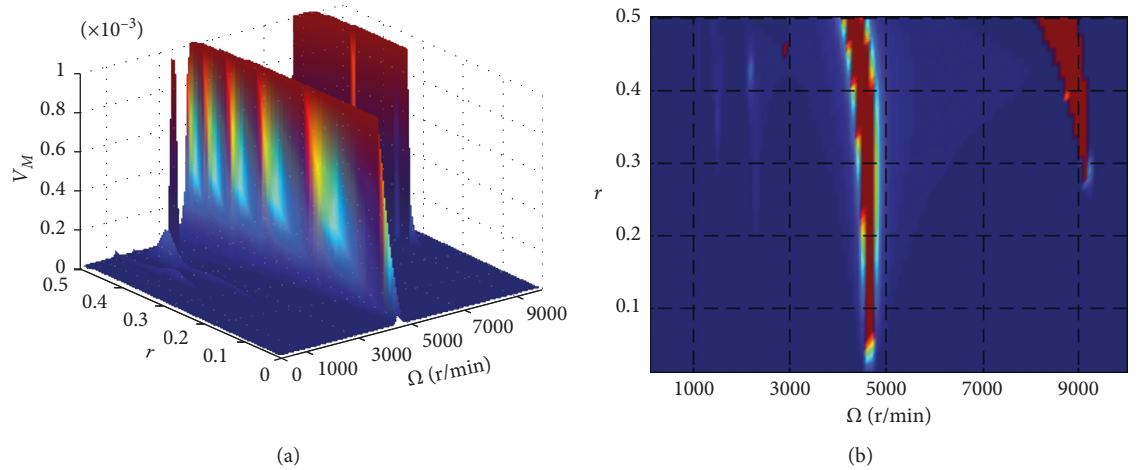

Figure 9: Average degrading rate versus crack depth ratio and rotation speed with $\varepsilon = 1 \times 10^{-5}$ m, $\beta = 1/2\pi$, and $\zeta = 0.01$.

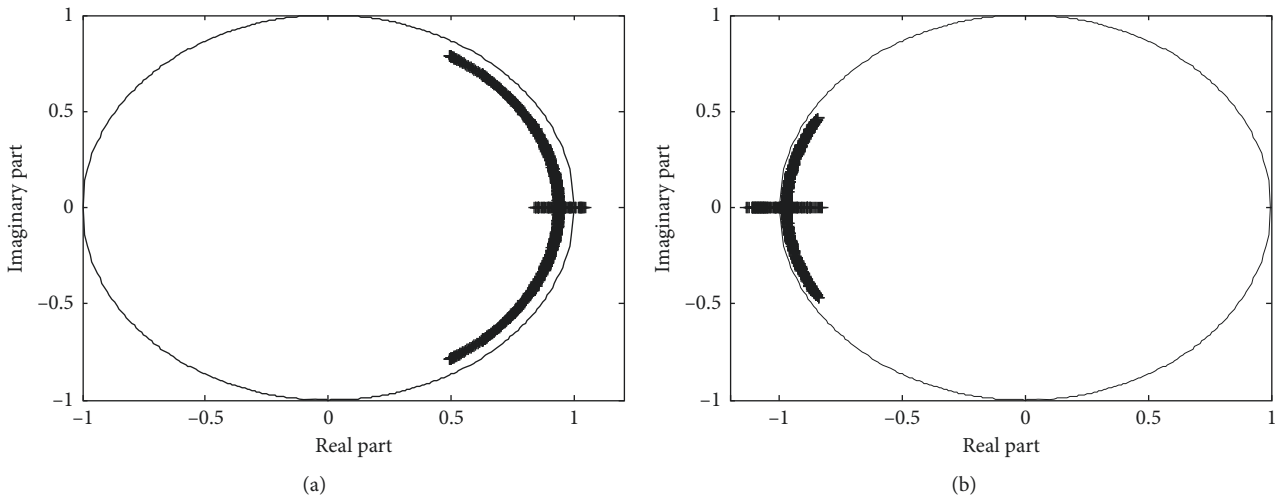

Figure 10: Floquet multipliers with r changing from 0 to 0.5 for (a) 4000 rpm–4600 rpm (period doubling) and (b) 8000 rpm–9100 rpm (saddle-node).

6.2. Effect of Unbalance. In engineering practice, unbalance eccentricity is inevitable due to manufacturing and assembly errors. The unbalance eccentricity and orientation angle are two crucial parameters for the cracked rotor, which are analyzed in the following two sections, respectively.

6.2.1. Effect of Unbalance Eccentricity. The unbalance eccentricity is usually very small, but the effect on vibration behavior cannot be ignored [16, 29]. Then, the vibration behavior affects the crack growth, so it is significant to study the effect of unbalance eccentricity on degradation behavior. Given $\beta = 1/2\pi$ and $\zeta = 0.01$, T_D for various rotation speeds and different unbalance eccentricities ($\varepsilon = 0.5 \times 10^{-5}$ m, 1×10^{-5} m, 1.5×10^{-5} m, and 2×10^{-5} m) are shown in Figure 12. For different unbalance eccentricities, the regularity between T_D and rotation speed is almost the same. When the rotation speed is very slow ($\Omega < 1800$ rpm), T_D for different unbalance eccentricities are nearly identical. However, as rotation speed increases, the larger the unbalance eccentricity is, the shorter the T_D is, owing to the larger amplitude of the vibration responses. Besides, around the critical speed and submultiples of it, the effect of unbalance eccentricity is relatively slight. However, around the rotation speeds far away from the resonance and subresonance regions, unbalance eccentricity has considerable influence on T_D.

Given $\beta = 1/2\pi$ and $\zeta = 0.01$, the average degradation rates of the cracked rotor for different eccentricities ($\varepsilon = 0.5 \times 10^{-5}$ m, 1×10^{-5} m, 1.5×10^{-5} m, and 2×10^{-5} m) are shown in Figure 13. The regions of relatively fast average degradation rate are almost the same for different eccentricities. As the eccentricity increases, the fast degradation region around the critical speed becomes larger, while that around submultiples and double of the critical speed barely changes. It is illustrated that eccentricity has little effect on the subresonance motion compared to the resonance.

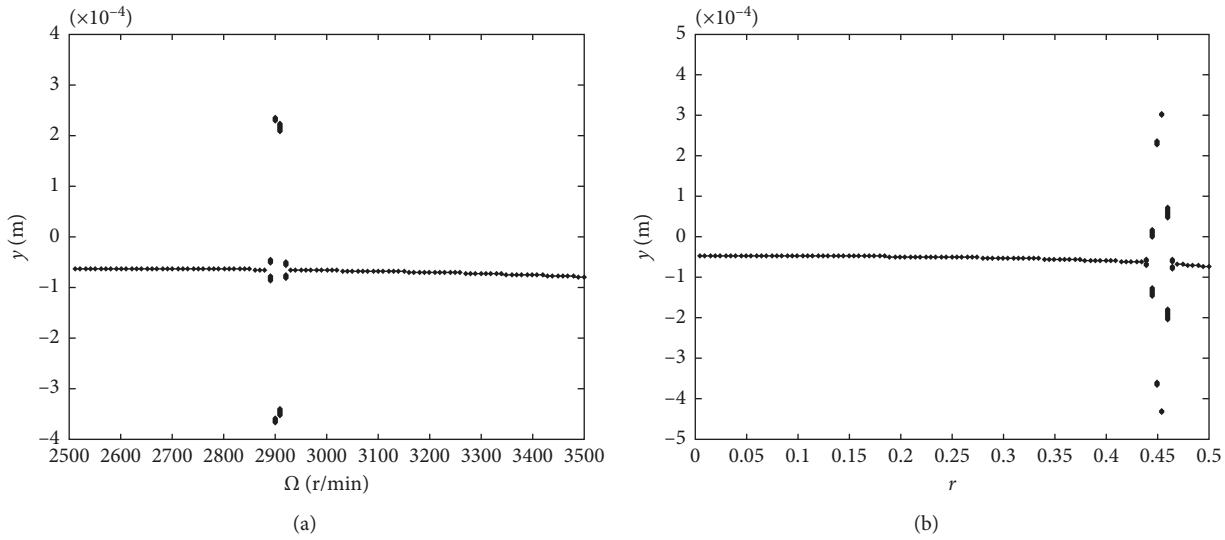

Figure 11: Bifurcation diagram for (a) $\Omega = 2500$ to 3500 rpm with $r = 0.45$, $\beta = 1/2\pi$, $\varepsilon = 1 \times 10^{-5}$ m, and $\zeta = 0.01$ and (b) r = 0 to 0.5 with $\Omega = 2900$ rpm, $\beta = 1/2\pi$, $\varepsilon = 1 \times 10^{-5}$ m, and $\zeta = 0.01$.

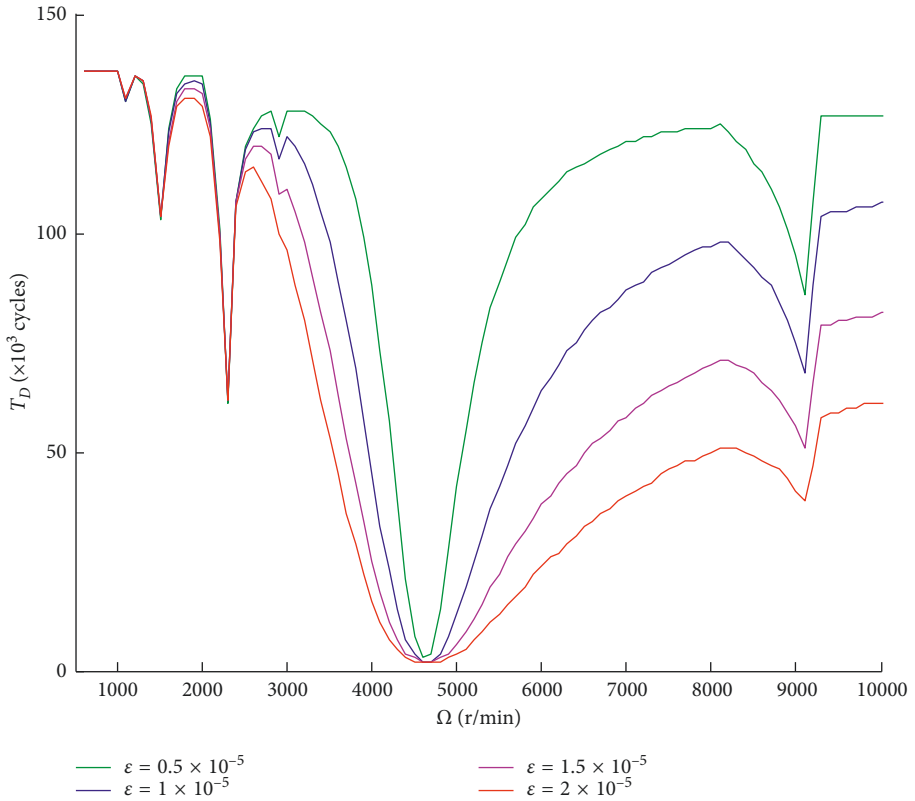

Figure 12: Fatigue degradation life versus rotation speed for various eccentricities with $\beta = 1/2\pi$ and $\zeta = 0.01$.

Around double of the critical speed, degradation failure occurs abruptly due to unstable vibration when crack depth reaches the threshold depth. Moreover, the judgment of this unstable vibration region has nothing to do with eccentricity with only the homogeneous form of the vibration differential equations considered according to Floquet's theory.

6.2.2. Effect of Unbalance Orientation Angle. The unbalance orientation angle is a crucial parameter having inescapable effect on vibration behavior of the cracked rotor, which has been studied by some researchers [16, 54–57]. Since the vibration is coupled with the crack growth, unbalance orientation angle affects the degradation behavior

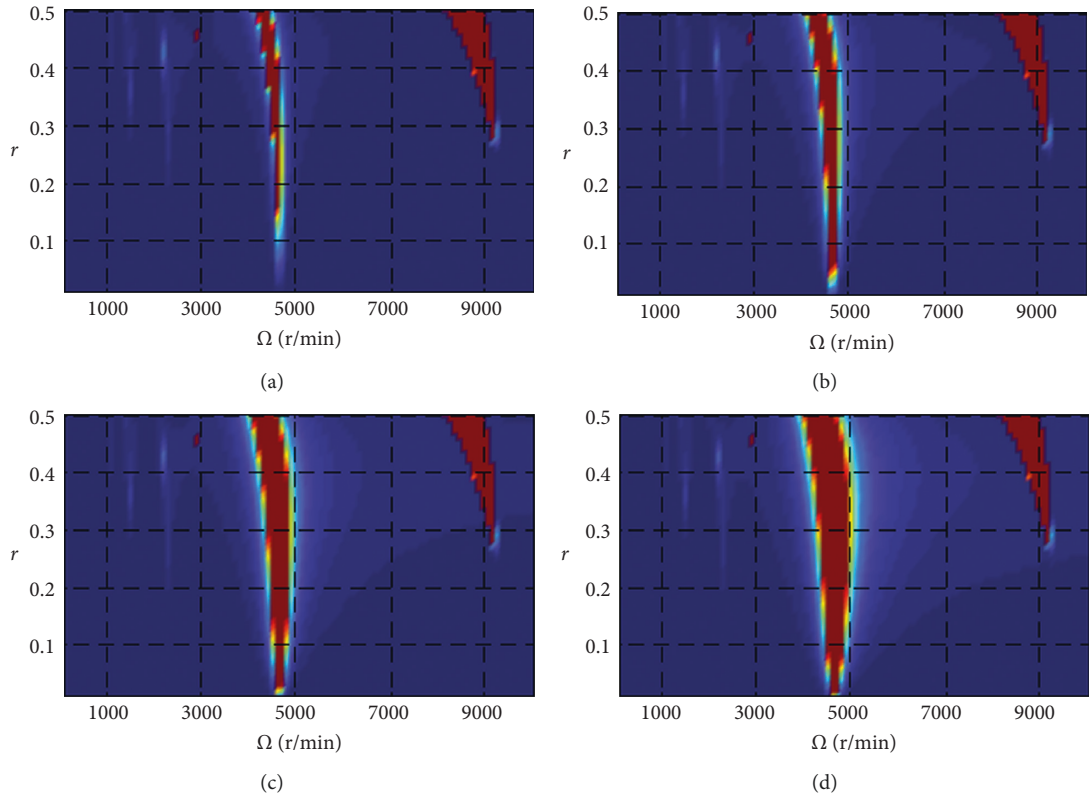

Figure 13: Average degrading rate versus crack depth ratio and rotation speed with $\beta = 1/2\pi$ and $\zeta = 0.01$ for various eccentricities: (a) $\varepsilon = 0.5 \times 10^{-5}$ m; (b) $\varepsilon = 1 \times 10^{-5}$ m; (c) $\varepsilon = 1.5 \times 10^{-5}$ m; (d) $\varepsilon = 2 \times 10^{-5}$ m.

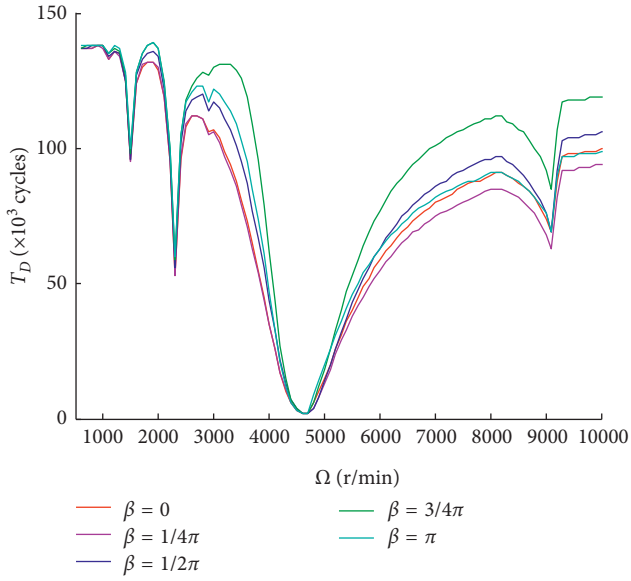

Figure 14: Fatigue degradation life versus rotation speed for various unbalance orientation angles with $\varepsilon = 1 \times 10^{-5}$ m and $\zeta = 0.01$.

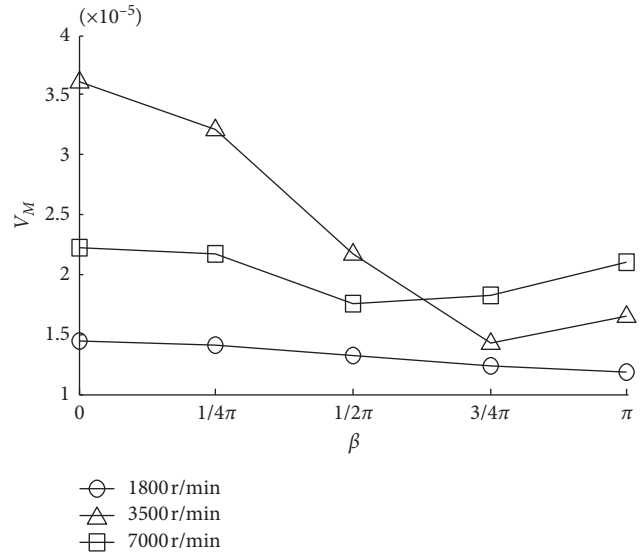

Figure 15: Average degradation rate versus unbalance orientation angle for different rotation speeds with $r = 0.4$, $\varepsilon = 1 \times 10^{-5}$ m, and $\zeta = 0.01$.

consequently. Given $\varepsilon = 1 \times 10^{-5}$ m and $\zeta = 0.01$, T_D for various rotation speeds and different unbalance orientation angles (0-π, with increment $1/4\pi$) are shown in Figure 14, noting that the case for $\beta \in (\pi, 2\pi)$ is omitted on the account of geometric symmetry. As shown in Figure 14, the regularity between T_D and rotation speed is almost the same for different β. Around the critical speed and submultiples of it, the effect of β is relatively slight. However, around the other rotation speeds, β has a considerable effect on T_D. It is worth noting that the speed range affected by the unbalance

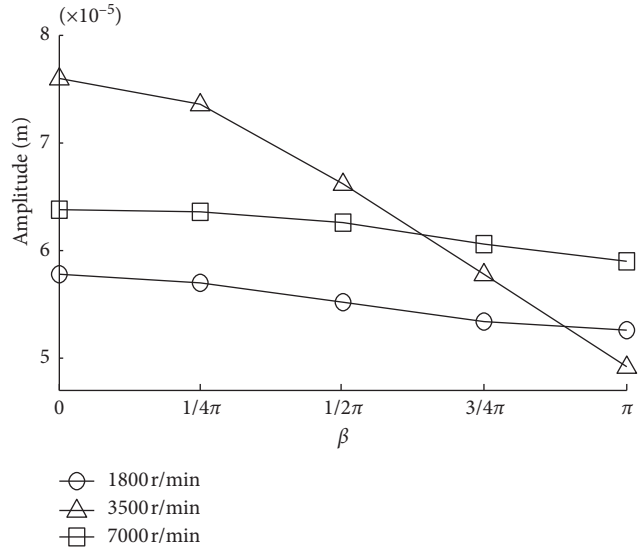

Figure 16: Vibration amplitude versus unbalance orientation angle for different rotation speeds with $r = 0.4$, $\varepsilon = 1 \times 10^{-5}$ m, and $\zeta = 0.01$.

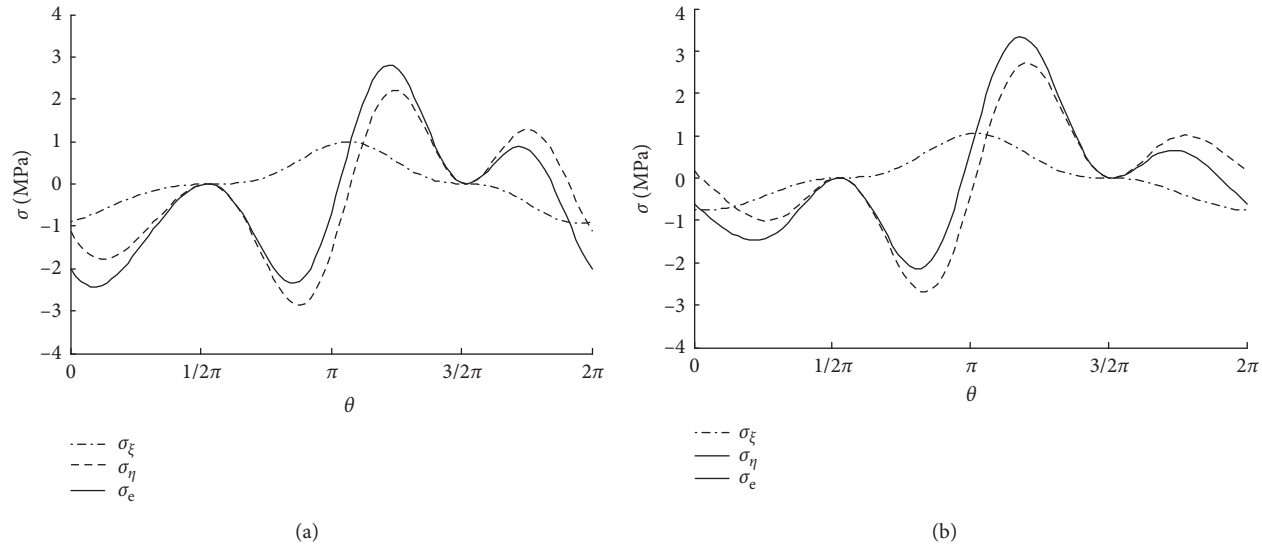

Figure 17: Stress variation during a rotation period with $\Omega = 7000$ rpm, $r = 0.4$, $\varepsilon = 1 \times 10^{-5}$ m, and $\zeta = 0.01$: (a) $\beta = 3/4\pi$; (b) $\beta = \pi$.

orientation angle is consistent with that affected by unbalance eccentricity.

When $\Omega > 2300$ rpm (1/2 of the critical speed), T_D is larger for $\beta = 3/4\pi$ and is smaller for $\beta = 1/4\pi$. However, when $\Omega < 2300$ rpm, T_D is larger for $\beta = \pi$. Take 1800 rpm, 3500 rpm, and 7000 rpm as representative rotation speeds to investigate the different effects of β for different speed ranges. Given $r = 0.4$, $\varepsilon = 1 \times 10^{-5}$ m, and $\zeta = 0.01$, the average degradation rates for different β are shown in Figure 15 and the amplitude of vibration response are shown in Figure 16. When $\Omega = 1800$ rpm, V_M decreases as β increases. However when $\Omega = 3500$ rpm and 7000 rpm, V_M decreases firstly and then increases as β increases. As to the vibration amplitude shown in Figure 16, the amplitude decreases as β increases for all the three speeds, and the amplitude is the smallest at $\beta = \pi$, which is in agreement with the result of [56, 57]. It is worth noting that when $\Omega = 3500$ rpm and 7000 rpm, the V_M increases as the amplitude decreases for relatively large β, which is different than anticipated. The reason is that different β causes different variation of the vibration phase [58] and then leads to the offset or superposition of the tensile or compressive stresses of the directions ξ and η. Therefore, the range of the equivalent stress may be inconsistent with the magnitude of the vibration amplitude. Given $\Omega = 7000$ rpm, $r = 0.4$, $\varepsilon = 1 \times 10^{-5}$ m, and $\zeta = 0.01$, the variation of σ_ξ, σ_η, and σ_e during one rotation period for $\beta = 3/4\pi$ and $\beta = \pi$ is shown in Figure 17. The different effects of $\beta = 3/4\pi$ and $\beta = \pi$ on the offset or

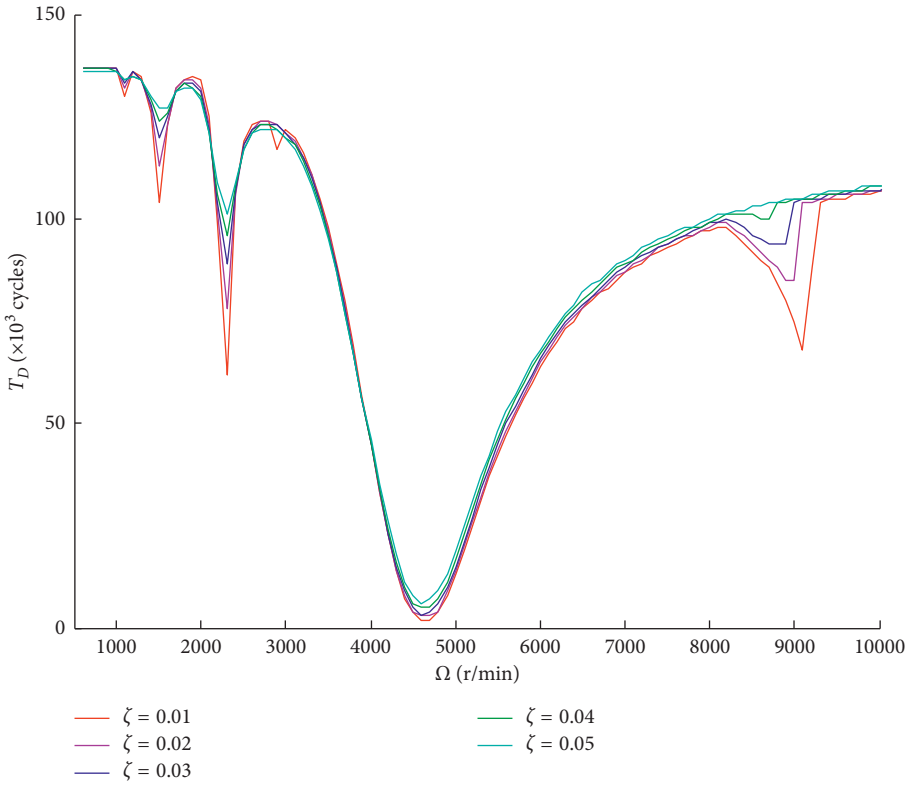

Figure 18: Fatigue degradation life versus rotation speed for various damping with $\varepsilon = 1 \times 10^{-5}$ m and $\beta = 1/2\pi$.

superposition of the stresses are not obviously presented in Figure 17 due to the very small variation of the stress during only one rotation period. However, for relatively large numbers of rotation periods, the effect becomes remarkable due to accumulation. For example, when $\Omega = 7000$ rpm, $r = 0.4$, $\varepsilon = 1 \times 10^{-5}$ m, and $\zeta = 0.01$, the crack grows 4.1168×10^{-4} m after 1000 rotation periods for $\beta = 3/4\pi$ and 4.7291×10^{-4} m for $\beta = \pi$.

6.3. Effect of Damping. Damping is unavoidable in mechanical systems in practice, which is also an important parameter of the cracked rotor system. Given $\varepsilon = 1 \times 10^{-5}$ m and $\beta = 1/2\pi$, T_D for different damping ratios (0.01–0.05 with increment 0.01) and various rotation speeds are shown in Figure 18. For different damping ratios, the regularity of T_D versus Ω is almost the same. The larger the damping ratio is, the larger the T_D is. The influence of ζ on T_D is mainly reflected around the submultiples and double of the critical speed. At 2/3 of the critical speed (2900 rpm), larger damping ($\zeta \geq 0.02$) prevents the unstable bifurcation motion and T_D does not decrease for large damping, which is in agreement with the result reported by Gasch [52]. It is worth noting that the rotation speed ranges affected by damping is quite different from that by unbalance. Therefore, in order to increase T_D of a rotor running at a specific speed in practice, the effectiveness of reducing unbalance or increasing damping should be carefully considered. Besides, the valley of T_D is vanished around double of the critical speed when damping is large ($\zeta = 0.05$). The reason is that degradation failure caused by unstable vibration response does not occur since the large damping prevents the bifurcation motion of the cracked rotor system.

Given $\varepsilon = 1 \times 10^{-5}$ m and $\beta = 1/2\pi$, the average degradation rates for different damping ratios ($\zeta = 0.02$, 0.03, 0.04, and 0.05) are shown in Figure 19. It is revealed that damping has obvious influence on the region of relatively fast degradation rate. As damping increases, each region of relatively fast degradation rate shrinks and the value of V_M decreases. Especially for large damping ($\zeta = 0.05$), the region of the fast degradation rate completely vanishes around double of the critical speed. The reason is that damping ratio ζ has great influence on the stability of the cracked rotor system. Specifically, the area of the unstable region decreases as damping ratio increases, which means damping is beneficial for the stability of the cracked rotor system [27, 37, 52, 53]. Given $\varepsilon = 1 \times 10^{-5}$ m and $\beta = 1/2\pi$, for different damping ratios ($\zeta = 0.01$ and 0.05), the 3D graphs of the maximum Floquet multipliers with the change of crack depth and rotation speed are shown in Figure 20. Moreover, the Floquet multipliers are plotted on the complex plane as also shown in Figure 20. For small damping ratio ($\zeta = 0.01$), the maximum Floquet multipliers exceed 1 around the critical speed and double of it with a deep crack ($r > 0.2$). The way in which the Floquet multipliers exceed the unit circle as shown in Figure 20(a) indicates the types of bifurcation for unstable vibration responses are period doubling and saddle-node. For large damping ratio ($\zeta = 0.05$), the maximum Floquet multipliers are always smaller than 1 as shown in Figure 20(b),

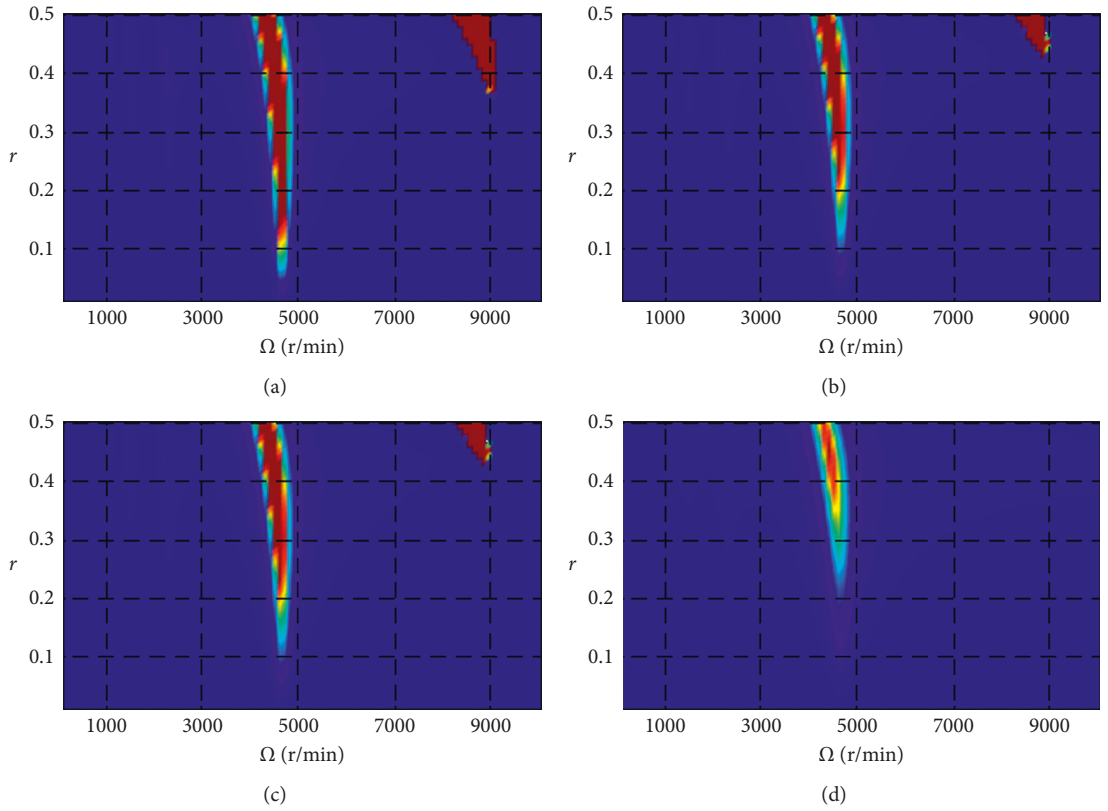

FIGURE 19: Average degrading rate versus crack depth ratio and rotation speed with $\varepsilon = 1 \times 10^{-5}$ m and $\beta = 1/2\pi$ for various damping ratios: (a) $\zeta = 0.02$; (b) $\zeta = 0.03$; (c) $\zeta = 0.04$; (d) $\zeta = 0.05$.

which means the vibration responses are stable for any crack depth and rotation speed labeled on the image.

7. Conclusions

The fast-slow coupling model of the rotor vibration and the crack growth is established, and an approximate numerical procedure based on sequential iteration is proposed to solve the coupling model. A competing degradation failure criterion is proposed through the analysis of the two degradation failure modes of the cracked rotor system, namely, crack rapid growth failure and unstable vibration failure. Numerical simulations show that if the coupling effect is omitted, one may obtain wrong degradation evolutions, which may cause risky accidents or waste of maintenance resources.

The effects of multiple parameters on the degradation behavior, including rotation speed, unbalance eccentricity and orientation angle, and damping, are investigated in detail. Results show that there is no simple intuitive regularity of degradation evolution, since the degradation behavior is affected by multiple parameters of the coupling model. When the rotation speed is around the critical speed, the vibration becomes unstable through period-doubling bifurcation, as the crack propagates. Due to the increase of vibration amplitude, the cracked rotor degrades very fast. When the rotation speed is around submultiples of the critical speed, degradation is relatively fast due to subresonance. And this phenomenon of fast degradation gradually vanishes as speed decreases. When the rotation speed is far away from the resonance and subresonance region, the degradation may also be fast due to the unstable vibration responses under some parameter group, for example, 2/3 of the critical speed with relatively deep crack and small damping. When the rotation speed is around double of the critical speed, the vibration may become unstable abruptly due to saddle-node bifurcation. Once the crack grows to some threshold depth, degradation failure occurs abruptly.

The degradation rate increases as unbalance eccentricity increases and as damping decreases. Unbalance orientation angle causes different variations of the vibration phase, which leads to the offset or superposition of the tensile or compressive stresses. Thus, when rotation speed is larger than 1/2 of the critical speed, degradation is slow for $\beta = 3/4\pi$; otherwise, degradation is slow for $\beta = \pi$. Moreover, the rotation speed ranges affected by damping are mainly the speed around the critical speed, submultiples, and double of it but that affected by unbalance eccentricity and orientation angle are just the opposite.

In engineering practice, the speed ranges corresponding to the fast fatigue degradation should be avoided and reducing unbalance eccentricity, changing unbalance orientation, or increasing damping can effectively retard

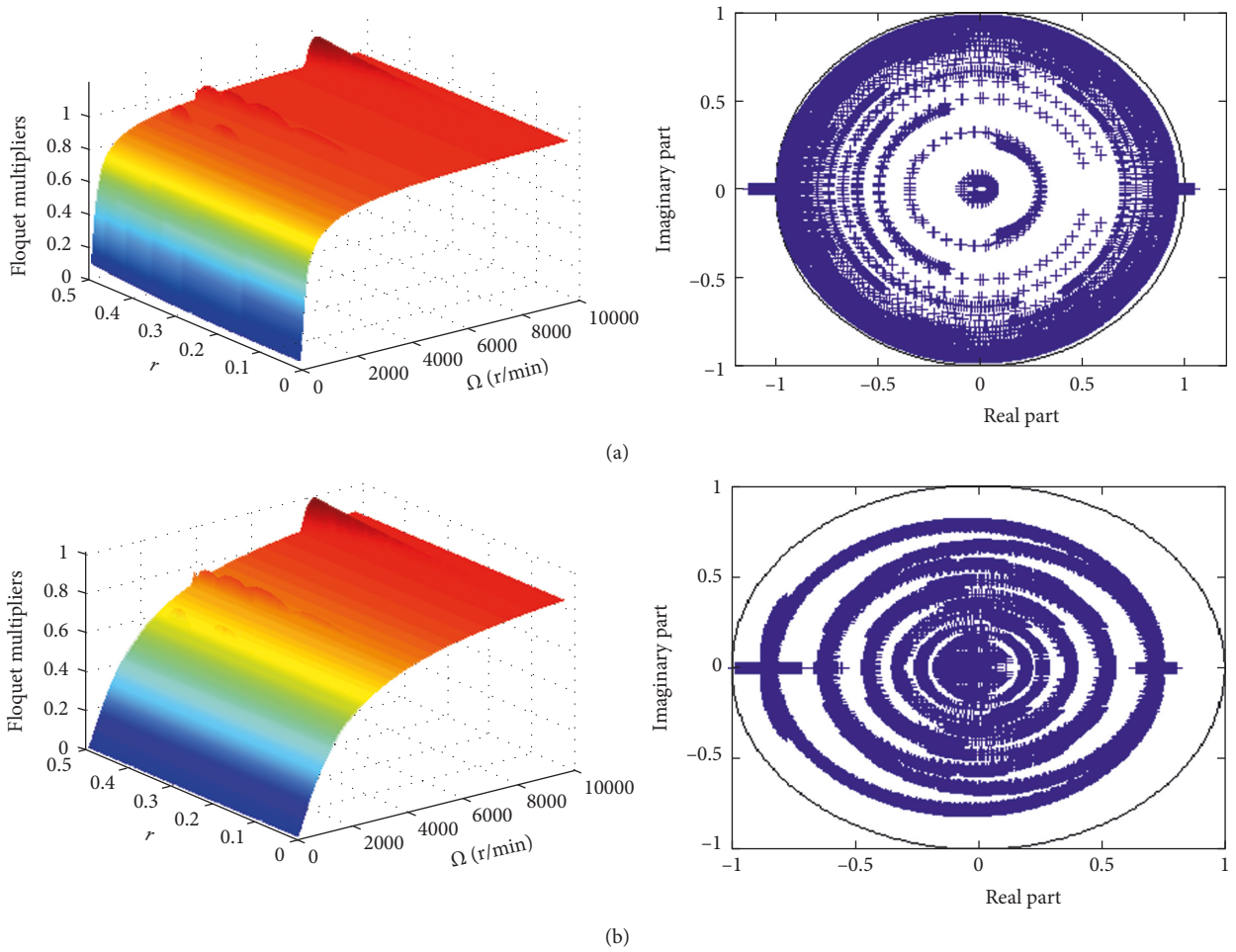

FIGURE 20: Maximum Floquet multipliers versus crack depth ratio and rotation speed and Floquet multipliers on the complex plane for (a) $\zeta = 0.01$ and (b) $\zeta = 0.05$.

degradation at specific rotation speeds. The findings are of significance to guide the safety design of the rotor system for long time operation and help to the further research on prognostics and lifetime prediction.

Appendix

A. Flexibility Coefficients of the Cracked Rotor

The total flexibility of the cracked rotor is made up of two parts: one is the uncracked rotor flexibility, and the other is the additional flexibility introduced by the crack. Based on the material mechanics, the uncracked rotor flexibility is

$$g_0 = \frac{L^3}{48EI}, \tag{A.1}$$

where L is the length of the shaft, E is Young's modulus, and I is the inertia moment of the shaft cross section, and $I = \pi D^2/64$.

The additional flexibility introduced by the crack changes with the amount of the open part of the crack. When accounting for partial opening and closing of the crack, the cross stiffness terms k_{xy} and k_{yx} appear. The flexibility due to crack is

$$g_{ij} = \frac{\partial u_i}{\partial Q_j}, \tag{A.2}$$

where i and j denote the direction of ξ and η, Q is the force acting on cross section of the crack, and u is the additional deflection due to the crack and is given as

$$u_i = \frac{\partial}{\partial Q_i}\left[\int J(\alpha)\, d\alpha\right]. \tag{A.3}$$

$J(\alpha)$ is the strain energy density function given by

$$J(\alpha) = \frac{1}{E}\left(K^I\right)^2. \tag{A.4}$$

K^I is the opening mode (mode I) stress intensity factors (SIFs), which is the sum of two SIFs:

$$K^I = K^I_{Q_\xi} + K^I_{Q_\eta}. \tag{A.5}$$

$K^I_{Q_\xi}$ and $K^I_{Q_\eta}$ are SIFs due to Q_ξ and Q_η, which are the lateral forces at the crack location. $K^I_{Q_\xi}$ and $K^I_{Q_\eta}$ are expressed as

$$K^I_{Q_\xi} = \sigma_\xi \sqrt{\pi\alpha} F\left(\frac{\alpha}{\alpha'}\right),$$
$$K^I_{Q_\eta} = \sigma_\eta \sqrt{\pi\alpha} F'\left(\frac{\alpha}{\alpha'}\right). \tag{A.6}$$

It may be noted that, owing to pure bending assumption, the effect of shear deformation is not taken into account. Also since torsional effects are not considered, cracking in modes II and III involving shear stresses is not present. σ_ξ and σ_η are the bending stress due to Q_ξ and Q_η, which are expressed as

$$\sigma_\xi(w) = \frac{\left(Q_\xi L/4\right)\left(\alpha'/2\right)}{I},$$
$$\sigma_\eta(w) = \frac{\left(Q_\eta L/4\right) w}{I}. \tag{A.7}$$

The functions F and F' in (9) are given by

$$F\left(\frac{\alpha}{\alpha'}\right) = \sqrt{\frac{2\alpha'}{\pi\alpha}\tan\left(\frac{\pi\alpha}{2\alpha'}\right)}\ \frac{0.923 + 0.199\left[1 - \sin\left(\pi\alpha/2\alpha'\right)\right]^4}{\cos\left(\pi\alpha/2\alpha'\right)}, \tag{A.8}$$

$$F'\left(\frac{\alpha}{\alpha'}\right) = \sqrt{\frac{2\alpha'}{\pi\alpha}\tan\left(\frac{\pi\alpha}{2\alpha'}\right)} \cdot \frac{0.752 + 2.02\left(\alpha/\alpha'\right) + 0.37\left[1 - \sin\left(\pi\alpha/2\alpha'\right)\right]^3}{\cos\left(\pi\alpha/2\alpha'\right)}. \tag{A.9}$$

Using (4)–(12), the flexibility coefficients of the cracked rotor can be written as

$$g_\xi = \frac{L^3}{48EI} + \iint \frac{128L^2\alpha'^2\alpha^2}{E\pi D^8} F\left(\frac{\alpha}{\alpha'}\right)^2 d\alpha\, dw,$$
$$g_\eta = \frac{L^3}{48EI} + \iint \frac{512L^2w^2\alpha}{E\pi D^8} F'\left(\frac{\alpha}{\alpha'}\right)^2 d\alpha\, dw,$$
$$g_{\xi\eta} = g_{\eta\xi} = \iint \frac{256L^2\alpha' w\alpha}{E\pi D^8} F\left(\frac{\alpha}{\alpha'}\right) F'\left(\frac{\alpha}{\alpha'}\right) d\alpha\, dw. \tag{A.10}$$

B. Stability Analysis Based on Floquet's Theory

Given $\mathbf{q} = [\, y \ \ x \,]^T$, (9) can be written as follows:

$$\mathbf{M}\ddot{\mathbf{q}} + \mathbf{C}\dot{\mathbf{q}} + \mathbf{K}(t)\mathbf{q} = \mathbf{F}, \tag{B.1}$$

where

$$\mathbf{M} = \begin{bmatrix} m & 0 \\ 0 & m \end{bmatrix},$$
$$\mathbf{C} = \begin{bmatrix} c & 0 \\ 0 & c \end{bmatrix},$$
$$\mathbf{F} = \begin{bmatrix} m\varepsilon\omega^2 \cos(\theta+\beta) - mg \\ m\varepsilon\omega^2 \sin(\theta+\beta) \end{bmatrix},$$
$$\mathbf{K} = \begin{bmatrix} \left\{k_0 - 0.5F(\theta)\left[2k_0 - \hat{k}_\xi - \hat{k}_\eta + \left(\hat{k}_\eta - \hat{k}_\xi\right)\cos 2\theta\right]\right\} & 0.5F(\theta)\left[\left(\hat{k}_\eta - \hat{k}_\xi\right)\sin 2\theta\right] \\ 0.5F(\theta)\left[\left(\hat{k}_\eta - \hat{k}_\xi\right)\sin 2\theta\right] & \left\{k_0 - 0.5F(\theta)\left[2k_0 - \hat{k}_\xi - \hat{k}_\eta - \left(\hat{k}_\eta - \hat{k}_\xi\right)\cos 2\theta\right]\right\} \end{bmatrix}. \tag{B.2}$$

According to Floquet's theory, the homogeneous form of (B.1) is considered, and the state space form is written as follows:

$$\dot{\mathbf{Y}} = \mathbf{A}(t)\mathbf{Y}, \tag{B.3}$$

where $\mathbf{Y} = [\, \dot{\mathbf{q}} \ \ \mathbf{q} \,]^T$.

$$\mathbf{A}(t) = \mathbf{A}(t+T) = \begin{bmatrix} -\mathbf{M}^{-1}\mathbf{C} & -\mathbf{M}^{-1}\mathbf{K} \\ \mathbf{I} & \mathbf{0} \end{bmatrix}, \tag{B.4}$$

where Hsu's approximate numerical method [45] is applied to calculate monodromy matrix $\mathbf{S}$. The rotation period T is divided into K intervals denoted by t_k, $0 < t_0 < t_1 < \cdots < t_k = T$, where the size of the kth interval is $\Delta_k = t_k - t_{k-1}$. In the kth interval, the periodic matrix $\mathbf{A}(t)$ is replaced by its averaged value, that is, by a constant matrix $\mathbf{C}_k$ defined by Hsu [45]:

$$\mathbf{C}_k = \frac{1}{\Delta_k}\int_{t_{k-1}}^{t_k} \mathbf{A}(t)\, dt. \tag{B.5}$$

The approximate monodromy matrix in the kth interval is expressed as

$$\mathbf{S}_k = e^{(\mathbf{C}_k\Delta_k)}, \tag{B.6}$$

and at the end of period T as

$$\mathbf{S} = \prod_{k=1}^{K}\mathbf{S}_k = \prod_{k=1}^{K} e^{(\mathbf{C}_k\Delta_k)}. \tag{B.7}$$

The matrix exponential $e^{(\mathbf{C}_k\Delta_k)}$ is difficult to calculate and can be evaluated by an N_lth-order truncated Taylor series:

$$e^{(\mathbf{C}_k\Delta_k)} \approx \mathbf{I} + \sum_{l=1}^{N_l} \frac{(\mathbf{C}_k\Delta_k)^l}{l!}. \tag{B.8}$$

Finally, the monodromy matrix $\mathbf{S}$ can be written as

$$\mathbf{S} \approx \prod_{k=1}^{K} \left[\mathbf{I} + \sum_{l=1}^{N_l} \frac{(\mathbf{C}_k\Delta_k)^l}{l!}\right]. \tag{B.9}$$

The eigenvalues $\mathbf{\Lambda} = \mathrm{eig}(\mathbf{S})$ of the monodromy matrix are called Floquet multipliers. According to Floquet's theory, if and only if the magnitudes of all its Floquet multipliers are less than one, that is, if

$$\max(|\mathbf{\Lambda}|) < 1, \tag{B.10}$$

the system is asymptotically stable.

Data Availability

The data used to support the findings of this study are available from the corresponding author upon request.

Conflicts of Interest

The authors declare that there are no conflicts of interest regarding the publication of this paper.

Acknowledgments

This work was partially supported by the National Natural Science Foundation of China (Grant nos. 51375434 and 51575497).

References

[1] J. Wauer, "On the dynamics of cracked rotors: a literature survey," *Applied Mechanics Reviews*, vol. 43, no. 1, pp. 13–17, 1990.

[2] A. D. Dimarogonas, "Vibration of cracked structures: a state of the art review," *Engineering Fracture Mechanics*, vol. 55, no. 5, pp. 831–857, 1996.

[3] C. A. Papadopoulos, "The strain energy release approach for modeling cracks in rotors: a state of the art review," *Mechanical Systems and Signal Processing*, vol. 22, no. 4, pp. 763–789, 2008.

[4] C. Kumar and V. Rostagi, "A brief review on dynamics of a cracked rotor," *International Journal of Rotating Machinery*, vol. 2009, Article ID 758108, 6 pages, 2009.

[5] L. M. Palacios-Pineda, J. C. Gómez-Mancilla, O. Martínez-Romero, and A. Elías-Zúñiga, "The influence of a transversal crack on rotor nonlinear transient response," *Nonlinear Dynamics*, vol. 90, no. 1, pp. 671–682, 2017.

[6] J. J. Sinou and A. W. Lees, "The influence of cracks in rotating shafts," *Journal of Sound and Vibration*, vol. 285, no. 4-5, pp. 1015–1037, 2005.

[7] C. A. Papadopoulous and A. D. Dimarogonas, "Coupled vibrations of cracked shafts," *Journal of Vibration and Acoustics*, vol. 114, no. 4, pp. 461–467, 1992.

[8] A. Ebrahimi, M. Heydari, and M. Behzad, "Forced vibration analysis of rotors with an open edge crack based on a continuous vibration theory," *Archive of Applied Mechanics*, vol. 87, no. 11, pp. 1871–1889, 2017.

[9] A. K. Darpe, K. Gupta, and A. Chawla, "Coupled bending, longitudinal and torsional vibrations of a cracked rotor," *Journal of Sound and Vibration*, vol. 269, no. 1-2, pp. 33–60, 2004.

[10] N. A. Saeed and M. Eissa, "Bifurcations of periodic motion of a horizontally supported nonlinear Jeffcott rotor system having transversely cracked shaft," *International Journal of Non-Linear Mechanics*, vol. 101, pp. 113–130, 2018.

[11] J. Pu, J. Chen, J. Zou, and P. Zhong, "The research on nonlinear characteristics of cracked rotor and reconstruction of crack forces," *Proceedings of Institution of Mechanical Engineers, Part C: Journal of Mechanical Engineering Science*, vol. 216, no. 11, pp. 1099–1108, 2002.

[12] J. Pu, J. Chen, J. Zou, and P. Zhong, "Quasi-periodic vibration of cracked rotor on flexible bearings," *Journal of Sound and Vibration*, vol. 251, no. 5, pp. 875–890, 2003.

[13] W. Qin, G. Meng, and T. Zhang, "The swing vibration, transverse oscillation of cracked rotor and the intermittence chaos," *Journal of Sound and Vibration*, vol. 259, no. 3, pp. 571–583, 2003.

[14] W. Qin, G. Chen, and X. Ren, "Grazing bifurcations in the response of cracked Jeffcott rotor," *Nonlinear Dynamics*, vol. 35, no. 2, pp. 147–157, 2004.

[15] F. Yiming, Z. Yufang, and Z. Shijian, "Analysis of the chaotic motion for the rotor system with transverse crack," *Acta Mechanica Solida Sinica*, vol. 16, pp. 74–80, 2003.

[16] T. H. Patel and A. K. Darpe, "Influence of crack breathing model on nonlinear dynamics of a cracked rotor," *Journal of Sound and Vibration*, vol. 311, no. 3–5, pp. 953–972, 2008.

[17] K. Suga, M. Kikuchi, Y. Wada, and H. Kawai, "Study on fatigue growth of multi-surface flaws in shaft under rotary bending by S-FEM," *Engineering Fracture Mechanics*, vol. 174, pp. 207–214, 2016.

[18] A. R. Maligno, S. Rajaratnam, S. B. Leen, and E. J. Williams, "A three-dimensional (3D) numerical study of fatigue crack growth using remeshing techniques," *Engineering Fracture Mechanics*, vol. 77, no. 1, pp. 94–111, 2010.

[19] N. Couroneau and J. Royer, "Simplified model for the fatigue growth analysis of surface cracks in round bars under mode I," *International Journal of Fatigue*, vol. 20, no. 10, pp. 711–718, 1998.

[20] F. P. Yang, Z. B. Kuang, and V. N. Shlyannikov, "Fatigue crack growth for straight-fronted edge crack in a round bar," *International Journal of Fatigue*, vol. 28, no. 4, pp. 431–437, 2006.

[21] K. Sobczyk and J. Trebicki, "Stochastic dynamics with fatigue-induced stiffness degradation," *Probabilistic Engineering Mechanics*, vol. 15, no. 1, pp. 91–99, 2000.

[22] J. Trebicki and K. Sobczyk, "On nonlinear stochastic vibratory systems with stiffness degradation," *Acta Mechanica*, vol. 195, no. 1–4, pp. 203–214, 2008.

[23] K. Sobczyk, K. Perros, and C. Papadimitriou, "Fatigue reliability of multidimensional vibratory degrading systems under random loading," *Journal of Engineering Mechanics*, vol. 136, no. 2, pp. 179–188, 2010.

[24] J. Luo, M. Namburu, K. Pattipati, L. Qiao, M. Kawamoto, and S. Chigusa, "Model-based prognostic techniques," in *Proceedings of IEEE AutoTestCon 2003*, Anaheim, CA, USA, September 2003.

[25] J. Luo, A. Bixby, K. Pattipati, L. Qiao, M. Kawamoto, and S. Chigusa, "An interacting multiple model approach to model-based prognostics," in *Proceedings of IEEE International Conference on Systems, Man and Cybernetics*, pp. 189–194, IEEE, Washington, DC, USA, October 2003.

[26] Y. Lei and W. Q. Zhu, "Fatigue crack growth in degrading elastic components of nonlinear structural systems under random loading," *International Journal of Solids and Structures*, vol. 37, no. 4, pp. 649–667, 2000.

[27] A. S. Sekhar and J. K. Dey, "Effects of cracks on rotor system instability," *Mechanism and Machine Theory*, vol. 35, no. 12, pp. 1657–1674, 2000.

[28] C. D. Untaroiu, A. Untaroiu, and M. Boiangiu, "Dynamic stability analysis of periodically time-varying rotor system with a transverse crack," *Engineering*, vol. 3, no. 7, pp. 719–725, 2011.

[29] P. Huichun, H. Qing, and Z. Yaxin, "Stability analysis of a breathing cracked rotor with imposed mass eccentricity," *Shock and Vibration*, vol. 2015, Article ID 453216, 17 pages, 2015.

[30] I. W. Mayes and W. G. R. Davies, "Analysis of the response of a multi-rotor-bearing system containing a transverse crack in a rotor," *Journal of Vibration, Acoustics, Stress, and Reliability in Design*, vol. 106, no. 1, pp. 139–145, 1984.

[31] J. E. T. P. Penny and M. I. Friswell, "Simplified modeling of rotor cracks," *Key Engineering Materials*, vol. 245, pp. 223–232, 2003.

[32] H. M. Mobarak, H. Wu, J. P. Spagnol, and K. Xiao, "New crack breathing mechanism under the influence of unbalance force," *Archive of Applied Mechanics*, vol. 88, no. 3, pp. 341–372, 2017.

[33] X. B. Lin and R. A. Smith, "Fatigue growth simulation for cracks in notched and unnotched round bars," *International Journal of Mechanical Sciences*, vol. 40, no. 5, pp. 405–419, 1998.

[34] P. Paris and F. Erdogan, "A critical analysis of crack propagation laws," *Journal of Basic Engineering*, vol. 85, no. 4, pp. 528–533, 1963.

[35] ASTM E647-15, *Standard Test Method for Measurements of Fatigue Crack Growth Rates*, American Society for Testing and Materials Standards, West Conshohocken, PA, USA, 2015.

[36] J. J. Sinou and A. W. Lees, "A non-linear study of a cracked rotor," *European Journal of Mechanics-A/Solids*, vol. 26, no. 1, pp. 152–170, 2007.

[37] C. Guo, M. A. AL-Shudeifat, J. Yan, L. A. Bergman, D. M. McFarland, and E. A. Butcher, "Stability analysis for transverse breathing cracks in rotor systems," *European Journal of Mechanics-A/Solids*, vol. 42, pp. 27–34, 2013.

[38] A. Ebrahimi, M. Heydari, and M. Behzad, "A continuous vibration theory for rotors with an open edge crack," *Journal of Sound and Vibration*, vol. 333, no. 15, pp. 3522–3535, 2014.

[39] Y. S. Shih and J. J. Chen, "Analysis of fatigue crack growth on a cracked shaft," *International Journal of Fatigue*, vol. 19, no. 6, pp. 477–485, 1997.

[40] A. Carpinteri, "Elliptical-arc surface cracks in round bars," *Fatigue and Fracture Engineering Material Structure*, vol. 15, no. 11, pp. 1141–1153, 1992.

[41] N. E. Dowling, "Fatigue failure predictions for complicated stress-strain histories," *Journal of Materials JMLSA*, vol. 7, pp. 71–87, 1972.

[42] M. Matsuishi and T. Endo, *Fatigue of Metals Subjected to Varying Stress*, Japan Society of Mechanical Engineers, Fukuoka, Japan, 1968.

[43] X. N. Zhang, Q. K. Han, Z. K. Peng, and F. L. Chu, "Stability analysis of a rotor–bearing system with time-varying bearing stiffness due to finite number of balls and unbalanced force," *Journal of Sound and Vibration*, vol. 332, no. 25, pp. 6768–6784, 2013.

[44] Z. Kulesza and J. T. Sawicki, "Damping by parametric excitation in a set of reduced-order cracked rotor systems," *Journal of Sound and Vibration*, vol. 354, pp. 167–179, 2015.

[45] C. S. Hsu, "On approximating a general linear periodic system," *Journal of Mathematical Analysis and Application*, vol. 45, no. 1, pp. 234–251, 1974.

[46] C. Feng and B. S. Kang, "Young's modulus measurement using a simplified transparent indenter measurement technique," *Experimental Mechanics*, vol. 48, no. 1, pp. 9–15, 2008.

[47] J. C. Huang and C. Bi, "A method for high precision spindle motor eccentricity measurement," in *Proceedings of Asia-Pacific Magnetic Recording Conference*, pp. 1–3, IEEE, Singapore, November-December 2006.

[48] L. Xu, "The damping iterative parameter identification method for dynamical systems based on the sine signal measurement," *Signal Processing*, vol. 120, pp. 660–667, 2016.

[49] D. Montalvão and J. M. M. Silva, "An alternative method to the identification of the modal damping factor based on the dissipated energy," *Mechanical Systems and Signal Processing*, vol. 54-55, pp. 108–123, 2016.

[50] M. Karkee and B. L. Steward, "Local and global sensitivity analysis of a tractor and single axle grain cart dynamic system model," *Biosystems Engineering*, vol. 106, no. 4, pp. 352–366, 2010.

[51] G. Meng and E. J. Hahn, "Dynamic response of a cracked rotor with some comments on crack detection," *Journal of Engineering for Gas Turbines and Power*, vol. 119, no. 2, pp. 447–455, 1994.

[52] R. Gasch, "Dynamic behavior of the Laval rotor with a transverse crack," *Mechanical Systems and Signal Processing*, vol. 22, no. 4, pp. 790–804, 2008.

[53] R. Gasch, M. Person, and B. Weitz, "Dynamic behavior of the Laval rotor with a cracked hollow shaft-a comparison of crack models," in *Proceedings of Institution of Mechanical Engineers Conference on Vibration in Rotating* Machinery, Edinburgh, UK, C314/88, UK, September 1988.

[54] A. K. Darpe, K. Gupta, and A. Chawla, "Transient response and breathing behavior of the cracked Jeffcott rotor," *Journal of Sound and Vibration*, vol. 272, no. 1-2, pp. 207–243, 2004.

[55] J. Schmied and E. Kramer, "Vibrational behavior of a rotor with a cross sectional crack," *Proceedings of Institution of Mechanical Engineers, Journal of Mechanical Engineering Science*, vol. 195, pp. 57–73, 1984.

[56] L. Cheng, N. Li, X. F. Chen, and Z. J. He, "The influence of crack breathing and imbalance orientation angle on the characteristics of the critical speed of a cracked rotor," *Journal of Sound and Vibration*, vol. 330, no. 9, pp. 2031–2048, 2011.

[57] Q. He, H. C. Peng, P. C. Zhai, and Y. X. Zhen, "The effects of unbalance orientation angle on the stability of the lateral torsion coupling vibration of an accelerated rotor with a transverse breathing crack," *Mechanical Systems and Signal Processing*, vol. 75, pp. 330–344, 2016.

[58] M. A. AL-Shudeifat, "On the finite element modeling of the asymmetric cracked rotor," *Journal of Sound and Vibration*, vol. 332, no. 11, pp. 2795–2807, 2013.

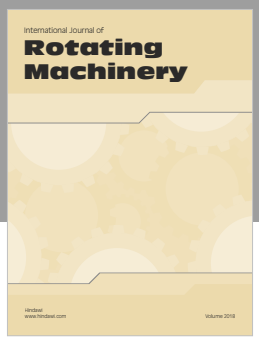

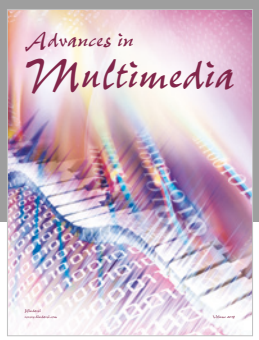

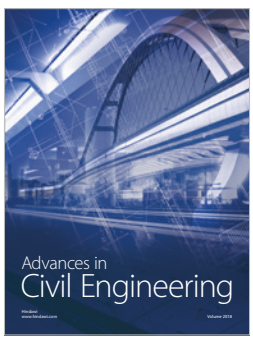

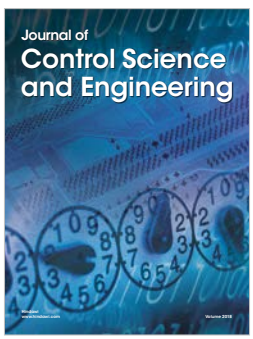

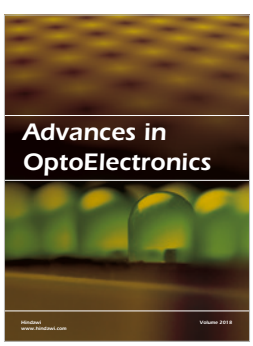

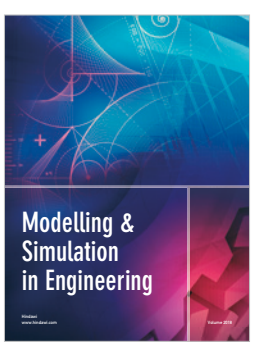

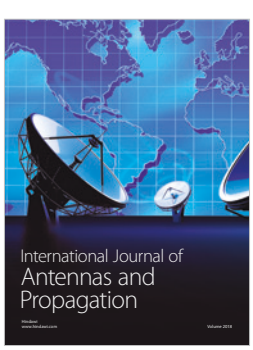

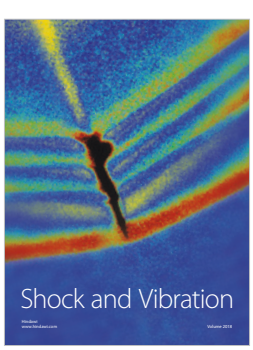

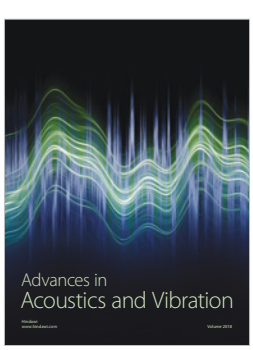

Hindawi

Submit your manuscripts at
www.hindawi.com